Please cite this article in press as: Tanimura et al., Hair Follicle Stem Cells Provide a Functional Niche for Melanocyte Stem Cells, Cell Stem Cell (2011), doi:10.1016/j.stem.2010.11.029

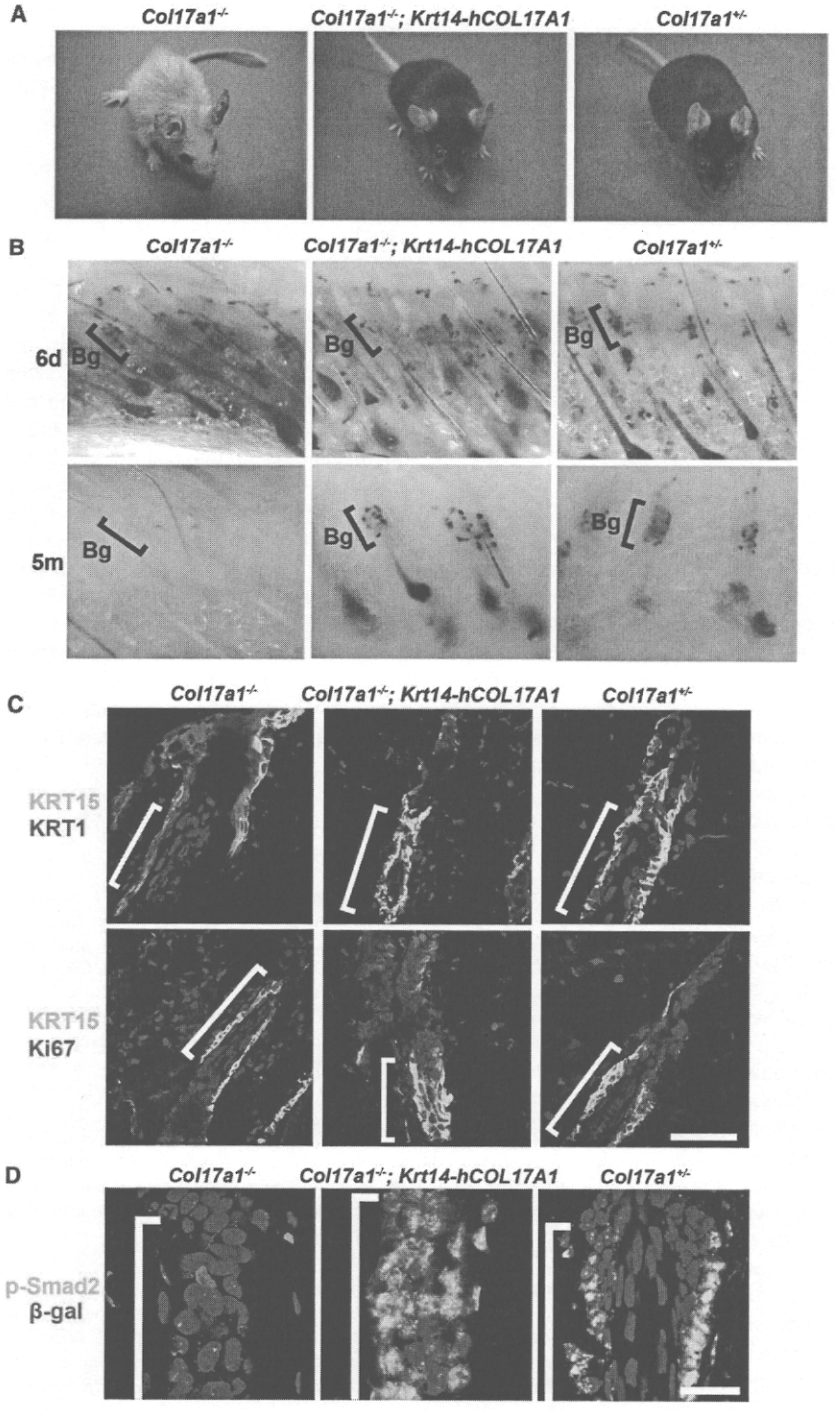

Figure 6. Transgene-Mediated Correction of *COL17A1* Expression in *Col17a1*$^{-/-}$ Basal Keratinocytes Rescues the Loss of MSCs

The *Krt14-hCOL17A1* transgene was introduced into *Col17a1*$^{-/-}$ mice.

(A) Macroscopic phenotype of 7- to 9-month-old *Col17a1*$^{-/-}$ mice with the *Krt14-hCOL17A1* transgene and *Col17a1*$^{+/-}$ mice.

(B) Distribution and morphology of *Dct-lacZ*-expressing melanoblasts in the bulge area (Bg) are normalized by the *Krt14-hCOL17A1* transgene in *Col17a1*$^{-/-}$ mice. Bulge-subbulge areas are demarcated by brackets.

(C) Ectopic KRT1 expression and abnormal proliferation of HFSCs in the bulge-subbulge area (brackets) are corrected by the *Krt14-hCOL17A1* transgene in *Col17a1*$^{-/-}$ mice. These mice were observed at 13 weeks of age during the anagen phase. Scale bar represents 50 μm.

(D) The downregulated expression of phospho-Smad2 (in green) in *Col17a1*$^{-/-}$ HFSCs and MSCs within the bulge-subbulge areas (demarcated by brackets) was also normalized by forced expression of the *Krt14-hCOL17A1* transgene in *Col17a1*$^{-/-}$ keratinocytes. Dct-lacZ-expressing melanocytes in the bulge area are shown in red. Scale bars represents 20 μm.

See also Figure S6.

with mechanical stress. Although mechanical stress, such as attempts to peel the neonatal mouse skin, can induce skin erosion or blistering in *Col17a1*-null mice (Nishie et al., 2007), it did not significantly accelerate hair graying or hair loss in these mice. Importantly, we did not find evidence of macroscopic/microscopic junctional separation, basal cell death, nor inflammatory cell infiltrates between the HFSCs and the basement membrane in *Col17a1*-null mouse skin. Instead, we found that significant defects in HFSC quiescence and immaturity in *Col17a1*-null mice were the earliest events that could explain the defective maintenance of HFSCs over ensuing hair cycles. These findings underline a critical cell-autonomous role for COL17A1 in the maintenance of HFSCs under physiological conditions. Although we did not detect adhesion defects of *Col17a1*-null keratinocytes on feeder cells used for colony assay in this study, weakening of cell attachment has been found with human cultured keratinocytes treated with COL17A1 antibody under vibration conditions (Iwata et al., 2009). One adhesion-based explanation for the premature HFSC depletion in *Col17a1*-deficient mice is that COL17A1-dependent anchoring of HFSCs to the basal lamina might regulate the quiescence and differentiation of HFSCs by modifying their division frequency and properties. Regardless of the precise mechanism involved, our findings reveal a potential mechanism for the hair loss (alopecia) seen with human *COL17A1* deficiency, which causes the nonlethal form of junctional epidermolysis bullosa, also known as generalized atrophic benign epidermolysis bullosa (GABEB) (McGrath et al., 1995; Nishie et al., 2007). It has been reported that the hair loss in GABEB patients is not always associated with

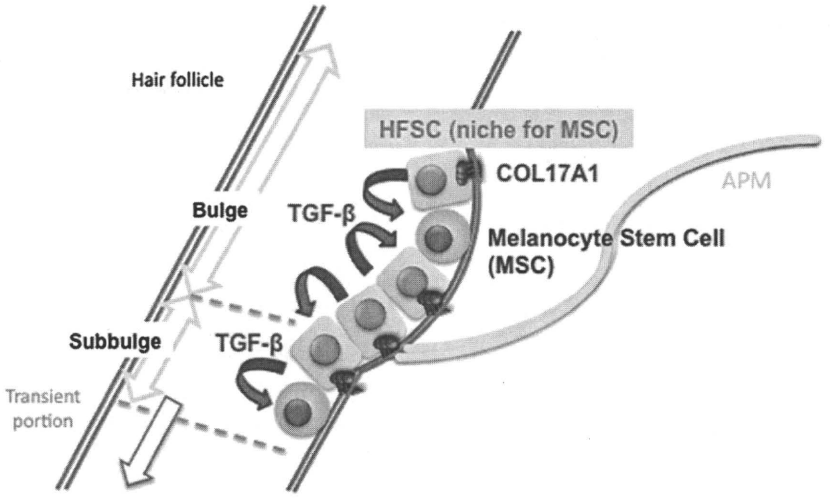

Figure 7. A Schematic Model for HFSCs and MSC Niche

HFSCs provide COL17A1-dependent niche for MSCs though TGF-β signaling. APM, arrector pili muscle.

surrounding skin surface changes but is associated with hair follicle atrophy or hair follicle loss (Hintner and Wolff, 1982). This finding is consistent with the late skin changes such as hair follicle atrophy seen in *Col17a1*-null mice. Therefore, we suggest that this mouse model may be a powerful tool for helping to understand the pathomechanisms of premature alopecia.

Human patients with GABEB also show epidermal atrophy with aging. *Col17a1*-deficient mice show transient epidermal hyperplasia in some focal areas at around 6 months of age (Figure 3D) but the entire skin becomes gradually more atrophic over time. Similar but more pronounced changes have been observed in the setting of stem cell depletion such as is seen in *Rac1* conditional knockout mice (Benitah et al., 2005) and in c-Myc transgenic mice (Arnold and Watt, 2001; Waikel et al., 2001). The late onset of epidermal atrophy seen in *Col17a1*-null mice might represent the eventual depletion or a decreased self-renewing potential of epidermal stem cells for the IFE.

More generally, *Col17a1*-null mice have provided evidence of an unexpected biological function for HFSCs. Although we have previously shown that the niche microenvironment plays a dominant role in fate determination for MSCs (Nishimura et al., 2002), the type of cell and/or the extracellular matrix in the bulge area that comprises the functionally essential component(s) of the niche has been unclear. Our current data indicate that HFSCs serve as a functional niche for MSCs and act through HFSC-derived TGF-β signaling, which is critical for MSC maintenance (Figure 7). It is notable that MSC immaturity was lost in *Col17a1*-deficient mice at a time when HFSCs were undergoing aberrant proliferation and differentiation in the bulge area with gradual loss of HFSC characteristics, including TGF-β production. There are a number of keratinocyte-specific gene-deficient mice that display a hair loss phenotype caused by HFSC depletion (Benitah et al., 2005; Zanet et al., 2005). However, as far as we know, characteristic premature hair graying has not been reported in those mice. It is also interesting that HFSCs nurture MSCs even though they are derived from a completely different developmental origin (Nishimura et al., 1999, 2002). A similar niche function provided by one type of stem cell for another was reported in *Drosophila melanogaster* testis and mouse bone marrow during the revision of this paper (Leatherman and Dinardo, 2010; Méndez-Ferrer et al., 2010; Omatsu et al., 2010). The maintenance of somatic stem cell populations in a coherent cell mass with a specialized tissue organization such as in the hair follicle bulge might be a recurring strategy for somatic stem cell maintenance. COL17A1 in the basal cell population of HFSCs (the α6-integrin^{high} population) (Blanpain et al., 2004) is critical not only for the maintenance of MSCs but also for the suprabasal HFSCs (α6-integrin^{low} population), which suggests a common niche function for basal HFSCs for the maintenance of adjacent MSCs and HFSCs. Further studies to elucidate the precise niche properties of HFSCs may clarify additional fundamental mechanisms for the maintenance of stem cell pools as clustered stem cell populations.

EXPERIMENTAL PROCEDURES

Animals

Dct-lacZ transgenic mice (Mackenzie et al., 1997) (a gift from I. Jackson), *Col17a1*-knockout mice (Nishie et al., 2007), and *Krt14*-human *COL17A1* transgenic mice (Olasz et al., 2007) have been described previously. *Col17a1*$^{+/+}$ and *Col17a1*$^{+/-}$ mice are referred to as control mice. *CAG-CAT-EGFP* mice (a gift from J. Miyazaki) were bred with *Dct*$^{tm1(Cre)Bee}$ mice (a gift from F. Beermann) to generate compound heterozygotes as described previously (Osawa et al., 2005). All mice were backcrossed to C57BL/6J. Animal experiments conformed to the Guide for the Care and Use of Laboratory Animals and were approved by the Institutional Committee of Laboratory Animal Experimentation.

TGF-βRII straight knockout mice (a gift from M. Taketo) (Oshima et al., 1996) were bred with Rag2-deficient mice at the Animal Research Facility of the Institute of Medical Science, University of Tokyo. Animal care of the line was carried out in accordance with the guidance of Tokyo University for animal and recombinant DNA experiments.

Histology, Immunohistochemistry, and Flow Cytometry Analyses

Paraffin, frozen sections, and whole-mount β-galactosidase staining were performed as previously described (Nishimura et al., 2002, 2005). Additional details on the methods and antibodies used are provided in the Supplemental Information. Multicolor flow cytometry analysis for HFSCs was performed with a FACSCalibur (BD).

Electron Microscopy

For electron microscopy, 20 μm cryostat sections were cut and stained in X-gal solution for 12 hr at 37°C. The sections were postfixed in 0.5% osmium tetroxide for 30 min, stained with 1% uranyl acetate for 20 min, dehydrated in a graded ethanol series, and then embedded in epoxy resin. Semithin sections (1 μm thick) were examined after toluidine blue staining and were observed by light microscopy. Ultrathin sections were observed with a JEM-1210 transmission electron microscope (JEOL) at 80 KV.

Isolation of Melanocytes

Dorsal skin was harvested from 6-day-old *CAG-CAT-EGFP/+; Dct$^{tml(Cre)Bee/\ tml(Cre)Bee}$* mice. The skin specimens were incubated in PBS containing 300 U/ml dispase (Sanko Junyaku) overnight at 4°C, and then the dermis was removed from the epidermis with a stereomicroscope. The epidermis was further dissociated by treatment with 0.25% trypsin for 10 min at 37°C. After neutralization with fetal calf serum (FCS), GFP$^+$ melanocytes were sorted with JSAN (Bay Bioscience).

RNA Isolation and Reverse Transcriptase Polymerase Chain Reaction

Total RNAs from mouse skin or sorted GFP$^+$ melanocytes were isolated with TRIzol (GIBCO) according to the manufacturer's instructions. 3 μg total RNA was used for cDNA synthesis in THERMOSCRIPT RT-PCR System (GIBCO) according to the manufacturer's instructions. The following primers were used for the analysis: mouse *Col17a1* (forward primer 5′-actcgcctcttcttca acca, reverse primer 5′-gagcaggacgccatgttatt) and *GAPDH* (forward primer 5′-accacagtccatgccatcac, reverse primer 5′-tccaccaccctgttgctgta).

Colony-Formation and Adhesion Assays

For the colony-forming assay, keratinocytes from newborn mice were used. Dorsal skins were incubated in PBS containing 300 U/ml dispase (Sanko Junyaku) for 1 hr at 37°C, after which the dermis was removed from the epidermis with a stereomicroscope. The epidermis was further dissociated by treatment with TrypLE Select (GIBCO) for 10 min at 37°C. The isolated cells (10^5 per 6 cm dish) were seeded on 3T3-J2 feeder cells treated with mitomycin C. The cells were grown in calcium-free medium (3:1 = calcium-free DMEM:CnT-57CF.S [Celltec]) supplemented with 1.8×10^{-4} M adenine, 1% antibiotic-antimyotic solution (Sigma), 2 mM L-glutamine, 0.5 μg/ml hydrocortisone, 5 μg/ml insulin, 10^{-10} M cholera enterotoxin, 10 ng/ml EGF, and 10% FCS treated with Chelex-100 resin (BioRad) at 32°C in a humidified atmosphere with 8% CO_2 for a total of 14 days. To visualize the keratinocyte colonies, the cells were washed with PBS and were then fixed in 4% formalin for 20 min at room temperature. After further washing in PBS, the cultures were stained for 5 min at room temperature with crystal violet.

For the adhesion assay, isolated keratinocytes (10^5 per well in 6-well plates) were seeded on 3T3-J2 feeder cells treated with mitomycin C or on collagen I-coated 6-well plates. 12 or 24 hr later, keratinocytes was washed three times in PBS and were collected with 0.05% trypsin-EDTA. Collected cells were fixed with 2% formaldehyde for 10 min at 37°C, permeabilized by ice-cold 100% methanol for 30 min, and stained with an Alexa Fluor 488-conjugated pan-cytokeratin monoclonal antibody (EXBIO). Detection of adherent keratinocytes was performed with a FACSCanto II (BD).

SUPPLEMENTAL INFORMATION

Supplemental Information includes Supplemental Experimental Procedures and six figures and can be found with this article online at doi:10.1016/j.stem.2010.11.029.

ACKNOWLEDGMENTS

We thank Dr. Makoto Taketo for *TGF-βRII* knockout mice; Dr. Hideki Nakamura, Dr. Tomohiko Wakayama, and Dr. Shoichi Iseki for their technical advice concerning electron microscopic analysis; Dr. Hiroyuki Nishimura for critical reading of the manuscript; Dr. Masashi Akiyama for discussion; Dr. Atsushi Hirao and Dr. Masako Ohmura for the use of the flow cytometer; Dr. Ken Natsuga for sample identification; and Ms. Misa Suzuki, Ms. Megumi Sato, and Ms. Yuika Osaki for technical assistance. This study was supported by grants from the Japanese Ministry of Education, Culture, Sports, Science, and Technology (17689033, 19390293), the Uehara Memorial Foundation, the Kato Memorial Bioscience Foundation, and the Takeda Science Foundation to E.K.N.

Received: May 13, 2009
Revised: July 27, 2010
Accepted: October 23, 2010
Published: February 3, 2011

REFERENCES

Arnold, I., and Watt, F.M. (2001). c-Myc activation in transgenic mouse epidermis results in mobilization of stem cells and differentiation of their progeny. Curr. Biol. *11*, 558–568.

Barrandon, Y., and Green, H. (1987). Three clonal types of keratinocyte with different capacities for multiplication. Proc. Natl. Acad. Sci. USA *84*, 2302–2306.

Benitah, S.A., Frye, M., Glogauer, M., and Watt, F.M. (2005). Stem cell depletion through epidermal deletion of Rac1. Science *309*, 933–935.

Blanpain, C., and Fuchs, E. (2006). Epidermal stem cells of the skin. Annu. Rev. Cell Dev. Biol. *22*, 339–373.

Blanpain, C., Lowry, W.E., Geoghegan, A., Polak, L., and Fuchs, E. (2004). Self-renewal, multipotency, and the existence of two cell populations within an epithelial stem cell niche. Cell *118*, 635–648.

Cotsarelis, G. (2006). Epithelial stem cells: A folliculocentric view. J. Invest. Dermatol. *126*, 1459–1468.

Darling, T.N., Bauer, J.W., Hintner, H., and Yancey, K.B. (1997). Generalized atrophic benign epidermolysis bullosa. Adv. Dermatol. *13*, 87–119, , discussion 120.

Dowling, J., Yu, Q.C., and Fuchs, E. (1996). Beta4 integrin is required for hemidesmosome formation, cell adhesion and cell survival. J. Cell Biol. *134*, 559–572.

Georges-Labouesse, E., Messaddeq, N., Yehia, G., Cadalbert, L., Dierich, A., and Le Meur, M. (1996). Absence of integrin alpha 6 leads to epidermolysis bullosa and neonatal death in mice. Nat. Genet. *13*, 370–373.

Greco, V., Chen, T., Rendl, M., Schober, M., Pasolli, H.A., Stokes, N., Dela Cruz-Racelis, J., and Fuchs, E. (2009). A two-step mechanism for stem cell activation during hair regeneration. Cell Stem Cell *4*, 155–169.

Green, H. (1977). Terminal differentiation of cultured human epidermal cells. Cell *11*, 405–416.

Guasch, G., Schober, M., Pasolli, H.A., Conn, E.B., Polak, L., and Fuchs, E. (2007). Loss of TGFbeta signaling destabilizes homeostasis and promotes squamous cell carcinomas in stratified epithelia. Cancer Cell *12*, 313–327.

Hintner, H., and Wolff, K. (1982). Generalized atrophic benign epidermolysis bullosa. Arch. Dermatol. *118*, 375–384.

Hojiro, O. (1972). Fine structure of the mouse hair follicle. J. Electron Microsc. (Tokyo) *21*, 127–138.

Inomata, K., Aoto, T., Binh, N.T., Okamoto, N., Tanimura, S., Wakayama, T., Iseki, S., Hara, E., Masunaga, T., Shimizu, H., and Nishimura, E.K. (2009). Genotoxic stress abrogates renewal of melanocyte stem cells by triggering their differentiation. Cell *137*, 1088–1099.

Iwata, H., Kamio, N., Aoyama, Y., Yamamoto, Y., Hirako, Y., Owaribe, K., and Kitajima, Y. (2009). IgG from patients with bullous pemphigoid depletes cultured keratinocytes of the 180-kDa bullous pemphigoid antigen (type XVII collagen) and weakens cell attachment. J. Invest. Dermatol. *129*, 919–926.

Leatherman, J.L., and Dinardo, S. (2010). Germline self-renewal requires cyst stem cells and stat regulates niche adhesion in *Drosophila* testes. Nat. Cell Biol. *12*, 806–811.

Li, L., and Xie, T. (2005). Stem cell niche: Structure and function. Annu. Rev. Cell Dev. Biol. *21*, 605–631.

Mackenzie, M.A., Jordan, S.A., Budd, P.S., and Jackson, I.J. (1997). Activation of the receptor tyrosine kinase Kit is required for the proliferation of melanoblasts in the mouse embryo. Dev. Biol. *192*, 99–107.

Masunaga, T., Shimizu, H., Yee, C., Borradori, L., Lazarova, Z., Nishikawa, T., and Yancey, K.B. (1997). The extracellular domain of BPAG2 localizes to anchoring filaments and its carboxyl terminus extends to the lamina densa of normal human epidermal basement membrane. J. Invest. Dermatol. *109*, 200–206.

McGrath, J.A., Gatalica, B., Christiano, A.M., Li, K., Owaribe, K., McMillan, J.R., Eady, R.A., and Uitto, J. (1995). Mutations in the 180-kD bullous pemphigoid antigen (BPAG2), a hemidesmosomal transmembrane collagen (COL17A1), in generalized atrophic benign epidermolysis bullosa. Nat. Genet. *11*, 83–86.

McMillan, J.R., Akiyama, M., and Shimizu, H. (2003). Epidermal basement membrane zone components: Ultrastructural distribution and molecular interactions. J. Dermatol. Sci. *31*, 169–177.

Méndez-Ferrer, S., Michurina, T.V., Ferraro, F., Mazloom, A.R., Macarthur, B.D., Lira, S.A., Scadden, D.T., Ma'ayan, A., Enikolopov, G.N., and Frenette, P.S. (2010). Mesenchymal and haematopoietic stem cells form a unique bone marrow niche. Nature *466*, 829–834.

Moore, K.A., and Lemischka, I.R. (2006). Stem cells and their niches. Science *311*, 1880–1885.

Morris, R.J., Liu, Y., Marles, L., Yang, Z., Trempus, C., Li, S., Lin, J.S., Sawicki, J.A., and Cotsarelis, G. (2004). Capturing and profiling adult hair follicle stem cells. Nat. Biotechnol. *22*, 411–417.

Nishie, W., Sawamura, D., Goto, M., Ito, K., Shibaki, A., McMillan, J.R., Sakai, K., Nakamura, H., Olasz, E., Yancey, K.B., et al. (2007). Humanization of autoantigen. Nat. Med. *13*, 378–383.

Nishimura, E.K., Yoshida, H., Kunisada, T., and Nishikawa, S.I. (1999). Regulation of E- and P-cadherin expression correlated with melanocyte migration and diversification. Dev. Biol. *215*, 155–166.

Nishimura, E.K., Jordan, S.A., Oshima, H., Yoshida, H., Osawa, M., Moriyama, M., Jackson, I.J., Barrandon, Y., Miyachi, Y., and Nishikawa, S. (2002). Dominant role of the niche in melanocyte stem-cell fate determination. Nature *416*, 854–860.

Nishimura, E.K., Granter, S.R., and Fisher, D.E. (2005). Mechanisms of hair graying: Incomplete melanocyte stem cell maintenance in the niche. Science *307*, 720–724.

Nishimura, E.K., Suzuki, M., Igras, V., Du, J., Lonning, S., Miyachi, Y., Roes, J., Beermann, F., and Fisher, D.E. (2010). Key roles for transforming growth factor beta in melanocyte stem cell maintenance. Cell Stem Cell *6*, 130–140.

Nishizawa, Y., Uematsu, J., and Owaribe, K. (1993). HD4, a 180 kDa bullous pemphigoid antigen, is a major transmembrane glycoprotein of the hemidesmosome. J. Biochem. *113*, 493–501.

Nowak, J.A., Polak, L., Pasolli, H.A., and Fuchs, E. (2008). Hair follicle stem cells are specified and function in early skin morphogenesis. Cell Stem Cell *3*, 33–43.

Olasz, E.B., Roh, J., Yee, C.L., Arita, K., Akiyama, M., Shimizu, H., Vogel, J.C., and Yancey, K.B. (2007). Human bullous pemphigoid antigen 2 transgenic skin elicits specific IgG in wild-type mice. J. Invest. Dermatol. *127*, 2807–2817.

Omatsu, Y., Sugiyama, T., Kohara, H., Kondoh, G., Fujii, N., Kohno, K., and Nagasawa, T. (2010). The essential functions of adipo-osteogenic progenitors as the hematopoietic stem and progenitor cell niche. Immunity *33*, 387–399.

Osawa, M., Egawa, G., Mak, S.S., Moriyama, M., Freter, R., Yonetani, S., Beermann, F., and Nishikawa, S. (2005). Molecular characterization of melanocyte stem cells in their niche. Development *132*, 5589–5599.

Oshima, M., Oshima, H., and Taketo, M.M. (1996). TGF-beta receptor type II deficiency results in defects of yolk sac hematopoiesis and vasculogenesis. Dev. Biol. *179*, 297–302.

Oshima, H., Rochat, A., Kedzia, C., Kobayashi, K., and Barrandon, Y. (2001). Morphogenesis and renewal of hair follicles from adult multipotent stem cells. Cell *104*, 233–245.

Paus, R., and Cotsarelis, G. (1999). The biology of hair follicles. N. Engl. J. Med. *341*, 491–497.

Paus, R., Müller-Röver, S., Van Der Veen, C., Maurer, M., Eichmüller, S., Ling, G., Hofmann, U., Foitzik, K., Mecklenburg, L., and Handjiski, B. (1999). A comprehensive guide for the recognition and classification of distinct stages of hair follicle morphogenesis. J. Invest. Dermatol. *113*, 523–532.

Powell, A.M., Sakuma-Oyama, Y., Oyama, N., and Black, M.M. (2005). Collagen XVII/BP180: a collagenous transmembrane protein and component of the dermoepidermal anchoring complex. Clin. Exp. Dermatol. *30*, 682–687.

Qiao, W., Li, A.G., Owens, P., Xu, X., Wang, X.J., and Deng, C.X. (2006). Hair follicle defects and squamous cell carcinoma formation in Smad4 conditional knockout mouse skin. Oncogene *25*, 207–217.

Raghavan, S., Bauer, C., Mundschau, G., Li, Q., and Fuchs, E. (2000). Conditional ablation of beta1 integrin in skin. Severe defects in epidermal proliferation, basement membrane formation, and hair follicle invagination. J. Cell Biol. *150*, 1149–1160.

Raymond, K., Deugnier, M.A., Faraldo, M.M., and Glukhova, M.A. (2009). Adhesion within the stem cell niches. Curr. Opin. Cell Biol. *21*, 623–629.

Tumbar, T., Guasch, G., Greco, V., Blanpain, C., Lowry, W.E., Rendl, M., and Fuchs, E. (2004). Defining the epithelial stem cell niche in skin. Science *303*, 359–363.

van der Neut, R., Krimpenfort, P., Calafat, J., Niessen, C.M., and Sonnenberg, A. (1996). Epithelial detachment due to absence of hemidesmosomes in integrin beta 4 null mice. Nat. Genet. *13*, 366–369.

Waikel, R.L., Kawachi, Y., Waikel, P.A., Wang, X.J., and Roop, D.R. (2001). Deregulated expression of c-Myc depletes epidermal stem cells. Nat. Genet. *28*, 165–168.

Watt, F.M. (2002). Role of integrins in regulating epidermal adhesion, growth and differentiation. EMBO J. *21*, 3919–3926.

Yang, L., Mao, C., Teng, Y., Li, W., Zhang, J., Cheng, X., Li, X., Han, X., Xia, Z., Deng, H., and Yang, X. (2005). Targeted disruption of Smad4 in mouse epidermis results in failure of hair follicle cycling and formation of skin tumors. Cancer Res. *65*, 8671–8678.

Yang, L., Wang, L., and Yang, X. (2009). Disruption of Smad4 in mouse epidermis leads to depletion of follicle stem cells. Mol. Biol. Cell *20*, 882–890.

Zanet, J., Pibre, S., Jacquet, C., Ramirez, A., de Alborán, I.M., and Gandarillas, A. (2005). Endogenous Myc controls mammalian epidermal cell size, hyperproliferation, endoreplication and stem cell amplification. J. Cell Sci. *118*, 1693–1704.

Journal of Dermatological Science 61 (2011) 38–44

Contents lists available at ScienceDirect

Journal of Dermatological Science

journal homepage: www.elsevier.com/jds

Expression of exon-8-skipped kindlin-1 does not compensate for defects of Kindler syndrome

Ken Natsuga [a,*], Wataru Nishie [a], Satoru Shinkuma [a], Hideki Nakamura [a], Yoichiro Matsushima [b], Aya Tatsuta [c], Mayumi Komine [c], Hiroshi Shimizu [a]

[a] Department of Dermatology, Hokkaido University Graduate School of Medicine, North 15 West 7, Sapporo, Japan
[b] Department of Dermatology, Sano Kosei General Hospital, Tochigi, Japan
[c] Department of Dermatology, Jichi Medical University, Tochigi, Japan

ARTICLE INFO

Article history:
Received 22 July 2010
Received in revised form 8 November 2010
Accepted 13 November 2010

Keywords:
Epidermolysis bullosa
Exon-trapping system
Basement membrane zone
Skin atrophy
Pseudo-ainhum

ABSTRACT

Background: Kindler syndrome (KS) is a rare, inherited skin disease characterized by blister formation and generalized poikiloderma. Mutations in *KIND1*, which encodes kindlin-1, are responsible for KS. c.1089del/1089+1del is a recurrent splice-site deletion mutation in KS patients.
Objective: To elucidate the effects of c.1089del/1089+1del at the mRNA and protein level.
Methods: Two KS patients with c.1089del/1089+1del were included in this study. Immunofluorescence analysis of KS skin samples using antibodies against the dermo-epidermal junction proteins was performed. Exon-trapping experiments were performed to isolate the mRNA sequences transcribed from genomic DNA harbouring c.1089del/1089+1del. β1 integrin activation in HeLa cells transfected with truncated *KIND1* cDNA was analyzed.
Results: Immunofluorescence study showed positive expression of kindlin-1 in KS skin with c.1089del/1089+1del mutation. We identified the exon-8-skipped in-frame transcript as the main product among multiple splicing variants derived from that mutation. HeLa cells transfected with *KIND1* cDNA without exon 8 showed impaired β1 integrin activation. Exon-8-coding amino acids are located in the FERM F2 domain, which is conserved among species, and the unstructured region between F2 and the pleckstrin homology domain.
Conclusion: This study suggests that exon-8-skipped truncated kindlin-1 is functionally defective and does not compensate for the defects of KS, even though kindlin-1 expression in skin is positive.

1. Introduction

Kindler syndrome (KS) is classified as a novel subtype of epidermolysis bullosa (EB) according to a revised classification of EB [1] and characterized by photosensitivity, skin fragility, fused fingers, and generalized progressive poikiloderma [2]. A characteristic histological finding in KS skin is the variability of epidermal separation and clefting at the epidermal basement membrane [3,4]. Former studies have confirmed that mutations in *COL7A1* are not a factor in KS patients [3,5].

In 2003, mutations in the *KIND1* gene encoding kindlin-1 were detected in KS patients [6,7]. The *KIND1* gene was mapped to chromosome 20p12.3 [7]. The gene spans 48.5 kb of genomic DNA and contains 14 coding sequences (exons 2–15) and one non-coding exon (exon 1) [2,7]. The *KIND1* gene is the human homolog of the *Caenorhabditis elegans* gene, *unc-112*, which encodes a membrane-associated structural/signaling protein that has been implicated in linking the actin cytoskeleton to the extracellular matrix (ECM) [7,8]. Kindlin-1 deficiency is associated with cutaneous basement membrane zone abnormalities and reduced integrin activation [9]. Also, kindlin-1 is necessary for lamellipodia formation *in vitro*, which is mediated by RhoGTPase signaling [10]. To date, more than 30 different loss-of-function mutations in *KIND1* have been reported [2].

Splicing is a common mRNA modification after transcription, in which introns are removed and exons are joined. This is mandatory for typical eukaryotic mRNA before it can be used to produce an accurate protein through translation. Nucleotide alterations in positions close to the spliced sites affect correct splicing of the mRNA transcript and result in complete skipping of the exon, retention of the intron, or the introduction of a new splice site

Abbreviations: KS, Kindler syndrome; ECM, extracellular matrix; EB, epidermolysis bullosa; SCC, squamous cell carcinoma; MASA, mutant-allele-specific amplification; PTC, premature termination codon; NMD, nonsense-mediated mRNA decay; PCR, polymerase chain reaction; DEJ, dermo-epidermal junction.

* Corresponding author. Tel.: +81 11 716 1161x5962; fax: +81 11 706 7820.
E-mail address: natsuga@med.hokudai.ac.jp (K. Natsuga).

0923-1811/$36.00
doi:10.1016/j.jdermsci.2010.11.008

within an exon or intron. Several methods are available to predict the consequences resulting from splice site mutations, such as the use of neural network software [11] (http://www.fruitfly.org/seq_tools/splice.html) and GeneSplicer software [12] (http://cbcb.umd.edu/software/GeneSplicer/). However, these programs cannot distinguish between pseudo and real splice sites [13]; therefore, other functional testing is necessary to correctly predict the mRNA products. Use of an exon-trapping system (Invitrogen, Carlsbad, CA) is one such approach for directly isolating transcribed mRNA sequences from genomic DNA [14]. This system is a reliable and easy-to-use tool for assessing the effects of splice-site mutations on mRNA splicing in cell cultures [15].

This study highlights a recurrent c.1089del/1089+1del in *KIND1* in KS patients. To elucidate the pathogenic effects of this deletion mutation on mRNA splicing, exon-trapping experiments were performed. We found that in-frame exon-8-skipped transcripts were produced by c.1089del/1089+1del defects. Immunofluorescence analysis of the patient's skin showed positive kindlin-1 staining, which might have resulted from exon-8-skipped kindlin-1. *In vitro* analysis using living cells revealed the expression of truncated kindlin-1 lead to impaired activation of β1 integrin. This study clarifies the complex sequelae resulting from a splice-site deletion mutation and provides greater understanding of the pathomechanisms involved in KS disease.

2. Materials and methods

2.1. Mutation detection

gDNA was extracted from the patient's peripheral blood cells. The mutation detection strategy was implemented after polymerase chain reaction (PCR) amplification of all exons and the intron–exon border of *KIND1*, followed by direct automated sequencing using an ABI Prism 3100 genetic analyzer (Advanced Biotechnologies, Columbia, MD). Oligonucleotide primers and PCR conditions used in this study are described elsewhere [7]. The genomic DNA nucleotides, the complementary DNA nucleotides, and the amino acids of the protein were numbered based on the following sequence information: GenBank accession no. NM_017671 [7].

2.2. Mutant-allele-specific amplification analysis

To verify the c.1761T>A mutation, using PCR products as a template, mutant-allele-specific amplification (MASA) analysis was performed with mutant-allele-specific primers carrying the substitution of two bases at the 3′-end mutant-allele-specific primers [16,17]: forward, 5′-ACATTCTGGGAGTTTCATGA-3′; reverse, 5′-CAATTCTGAGGGACACACAT-3′. Only the 179-bp fragment derived from the mutant allele was amplified with these primers.

2.3. Electron microscopy

Electron microscopy was performed as previously described [18,19]. Briefly, skin biopsy samples were fixed in 2% glutaraldehyde solution, post-fixed in 1% OsO_4, dehydrated, and embedded in Epon 812. The samples were sectioned at 1 μm thickness for light microscopy and thin sectioned for electron microscopy (70 nm thick). The thin sections were stained with uranyl acetate and lead citrate, and examined in a transmission electron microscope.

2.4. Antibodies

The following antibodies (Abs) were used: monoclonal antibody (mAb) HD1-121 against the rod domain of plectin; mAbs GoH3 and 3E1 against α6 and β4 integrins, respectively (Chemicon International, CA); mAb GB3 against laminin 332 (Sera-lab, Cambridge, UK); mAb LH7.2 against type VII collagen (Sigma, St. Louis, MO); mAb PHM-12+CIV22 against type IV collagen (NeoMarkers, Fremont, CA); S1193 against BP230; mAb HDD20 against type XVII collagen; anti-kindlin-1 Ab (ab68041) that recognizes the C-terminus of kindlin-1 (Abcam, Cambridge, UK); unconjugated and horseradish peroxidase conjugated anti-V5 Abs (Invitrogen); and mAbs 4B7R and 12G10 against β1 integrin (Abcam, Cambridge, UK). The following secondary antibodies were used: fluorescein isothiocyanate (FITC)-conjugated goat anti-rabbit Ab (Jackson Immuno Research, West Grove, PA); FITC-conjugated goat anti-mouse Ab (Jackson Immuno Research); and TIRTC-conjugated goat anti-mouse Ab (SouthernBiotech, Birmingham, AL); horseradish peroxidase-conjugated goat anti-mouse Ab (Jackson Immuno Research). mAb GoH3 was a kind gift from Dr. A. Sonnenberg of the Netherlands Cancer Institute. mAbs HD1-121 and HDD20 were kind gifts from Dr. K. Owaribe of Nagoya University. The antibody S1193 was a kind gift from Dr. J.R. Stanley of the University of Pennsylvania.

2.5. Skin immunofluorescence studies

Indirect immunofluorescence analysis using a series of antibodies against antigens at the dermo-epidermal junction (DEJ) and cryostat skin sections was performed as previously described [3,20].

2.6. Exon-trapping experiments

Exon-trapping (Invitrogen, Carlsband, CA) is an approach used for the direct isolation of mRNA sequences transcribed from gDNA. To generate a *KIND1* genomic fragment extending from intron 6 to intron 9, we synthesized two primers (5′-GAATTCCTGAGCTGAAGTTTGCTGCA-3′ and 5′-GGATCCACCTTTGAACCATGAACCTG-3′) which contained the respective restriction enzyme sites: EcoRI and BamHI. PCR were performed using the patient's gDNA as a template. The DNA fragment was digested with EcoRI and BamHI and subcloned into the multi-cloning site of a pSPL3 expression vector, which contained a portion of the HIV-1 tat gene, an intron, splice donor and acceptor sites, and some flanking exon sequences. Sequence analysis selected constructs with or without the splice site mutation c.1089del/c.1089+1del. The constructs were transfected into HaCaT cells using lipofectamine LTX (Invitrogen) according to the manufacturer's instructions. Total RNA was extracted from the cultured cells and RT-PCR was performed using the trapping vector-specific oligonucleotide primers. The samples without transfection of the SPL3 were used as controls. The PCR products were subcloned into a TA cloning vector pCRII (Invitrogen).

2.7. In vitro analysis of truncated KIND1

cDNA containing the entire coding region of *KIND1* (FEMT1wt) was subcloned into the pcDNA3.1V5-His vector (Invitrogen). *KIND1* cDNA without exon 8 was subcloned to generate the same vector minus exon 8 (KIND1delex8) using PCR methods and the following flanking *KIND1* cDNA primers: sense, 5′-GAGGACATTACTGATATCCC-3′, anti-sense, 5′-CTGTAGAGCTGCAAAGATCA-3′. Two different KIND1wt and KIND1delex8 transfections were performed into HeLa cells, using Lipofectamine LTX (Invitrogen). For immunoblotting, HeLa cells 24 h after transfection were lysed in Laemmli buffer [21], cell debris was removed by centrifugation, and supernatant was collected. SDS-PAGE and immunoblotting were performed using standard techniques. For immunofluorescence, HeLa cells at 24 h after transfection were washed with phosphate-buffered saline and fixed with methanol. All cells were observed using a confocal laser scanning microscope (Olympus Fluoview FV300).

The medical ethics committee of Hokkaido University approved all described studies. The study was conducted according to Declaration of Helsinki Principles. The patients gave their written informed consent.

3. Results

3.1. Case description

Patient 1 was a 40-year-old Japanese male. He was the first child of non-consanguineous, healthy parents. Generalized skin fragility had been seen since infancy and early childhood. Physical examination revealed extensive poikiloderma with reticular pigmentation involving the entire skin surface (Fig. 1a). Pseudo-ainhum was noted on the left middle, ring and small fingers (Fig. 1b). He developed cutaneous squamous cell carcinoma (SCC) on his right palm at the age of 27. A wide local excision was performed on the SCC, but the carcinoma recurred four times (Fig. 1c) and was treated with additional local excision and radiation therapy.

Ultrastructural observation of the skin specimen from Patient 1 revealed scattered lamina densa reduplication (Fig. 1d). The ultrastructural appearance of the basal lamina, including the anchoring fibrils and hemidesmosomes, was normal (Fig. 1d).

3.2. Recurrent c.1089del/1089+1del KIND1 mutation in Japanese KS patients

KIND1 mutation analysis revealed that Patient 1 was compound heterozygous for c.1761T>A (p.Tyr587X) (Fig. 2a) and c.1089del/1089+1del (Fig. 2b). Mutant-allele-specific amplification (MASA) analysis demonstrated that a 179-bp fragment derived from the mutant allele containing c.1761T>A was amplified from the patient's gDNA, but not from the DNA of normal controls (Fig. 2c). c.1089del/1089+1del was confirmed by TA-cloning (Fig. 2d). c.1761T>A (p.Tyr587X) was novel, and c.1089del/1089+1del had been described in two unrelated Japanese KS patients, who were homozygotes for that mutation [7].

3.3. Kindlin-1 expression in KS skin with c.1089del/1089+1del

Kindlin-1 labelling of Patient 1's skin showed linear staining at the DEJ with weak labelling at the cell periphery in the basal keratinocytes (Fig. 3a), which was not distinctly different from normal human skin (Fig. 3i). Skin specimens from another Japanese KS patient (Patient 2), who is homozygous for c.1089del/1089+1del, revealed the same kindlin-1 labelling pattern (Fig. 3e). Patient 2 was described in previous reports [3,7]. Briefly, she was a 38-year-old Japanese female with a history of photosensitivity, blister formation, fusion of the fingers, and esophageal and vaginal stenosis. Her clinical manifestation was extensive poikiloderma involving the entire skin surface [3].

Skin specimens from Patient 1 showed a thin linear expression pattern for all basement membrane proteins including α6 and β4 integrins, plectin, BP230, and type XVII collagen, using specific antibodies (data not shown). Laminin 332, type IV collagen and type VII collagen also revealed a thin linear labelling pattern (Fig. 3b–d). None of the immunohistochemical findings of interrupted or reduplicated dermo-epidermal junction that characterize typical KS were seen (Fig. 3b–d). On the other hand, laminin 332, type IV and VII collagen labelling of skin specimens from Patient 2 showed typical dermo-epidermal junction interruption, as previously described [3] (Fig. 3f–h).

3.4. In-frame skipping of exon 8 resulting from c.1089del/1089+1del

c.1089del/1089+1del was located at the splicing cryptic site. To analyse the transcripts resulting from c.1089del/1089+1del, a previously reported exon-trapping system was used [22,23]. We inserted the genomic fragments with or without c.1089del/1089+1del mutation into the pSPL3 vector, transfected these constructs into HaCaT cells and prepared total RNA from the cells. We then synthesized cDNA and amplified the extracted exons by PCR using vector-specific primers. PCR products were subcloned into TA-vector and sequenced. Sequence analysis revealed that all

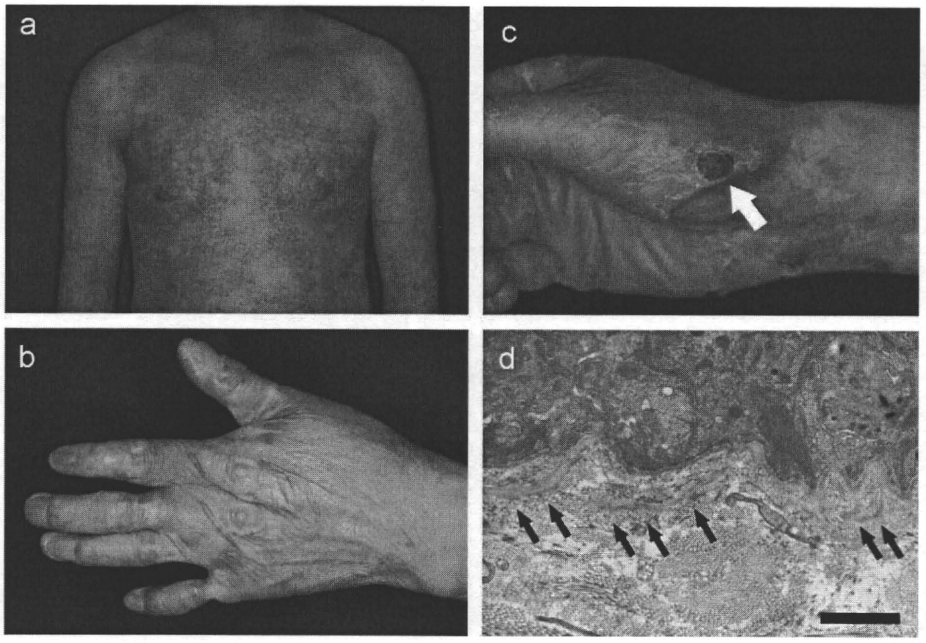

Fig. 1. Clinical and ultrastructural features of Patient 1. (a) Generalized poikiloderma is observed. (b) Pseudo-ainhum is seen from the left middle to little fingers. The middle and ring fingers are partly fused. (c) Recurrent squamous cell carcinoma (arrow) on the right palm at the age of 38. (d) Ultrastructural features of the skin specimens from Patient 1. Epidermal–dermal separation is not observed. Some reduplication of lamina densa is seen (arrows). No apparent abnormalities in hemidesmosomes and anchoring fibrils are detected (bar: 5 μm).

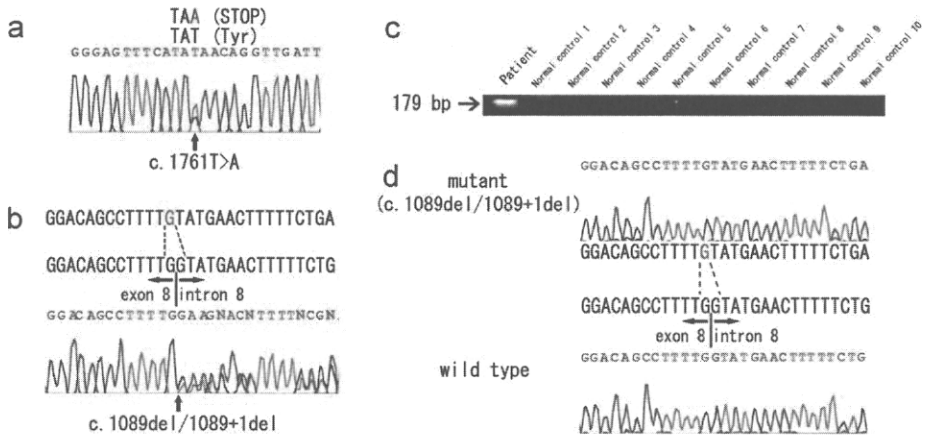

Fig. 2. *KIND1* mutation analysis of Patient 1. (a, b) Patient 1 is compound heterozygous for c.1761T>A (a) and c.1089del/1089+1del (b). An adenine that has replaced a thymine is indicated in red in the former mutation. A guanine deleted from two guanines at the exon 8–intron 8 boundary is indicated in red in the latter mutation. (c) Mutant-allele-specific amplification (MASA) analysis on c.1761T>A shows the amplification band from the mutant allele to be a 179-bp fragment from the patient's DNA sample, but no amplification was detected in normal controls. (d) TA-cloning of the PCR products derived from the patient's gDNA reveals wild-type (lower) and mutant (c.1089del/1089+1del, upper) subclones.

the clones without the mutation contained exons 7, 8 and 9 (wild-type transcript, Fig. 4a). The sequenced clones with the mutation showed six different transcripts (51 clones, transcripts 1–6, Fig. 4b–g). In most of the clones with the mutation (45 of 51 clones), skipping of exon 8 was observed (transcript 1, Fig. 4b). The size of exon 8 was 132 bp, so the deletion of exon 8 did not alter the coding frame and restored the translation of a polypeptide that was encoded by the downstream exons (Fig. 4b). In transcript 2 (1 of 51 clones), an exonic guanine deletion was seen at the 3′ end of exon 8, resulting in a frameshift followed by a premature termination codon (PTC) (Fig. 4c). A new splice donor site within intron 8, between nucleotides (nts) 1089 + 240 and 1089 + 241, was activated in transcript 3 (1 of 51 clones), also resulting in a frameshift and a subsequent PTC (Fig. 4d). In transcripts 4 and 5 (2 and 1 of 51 clones, respectively), two new splice donor sites within exon 8, between nts 1006 and 1007 and between nts 1066 and 1067, respectively, were activated, leading to a frameshift and a subsequent PTC (Fig. 4e and f). In transcript 6 (2 of 51 clones), the duplication of nts 1065–1066 (AG) compensated transcript 5, which did not alter the coding frame and restored the translation of a polypeptide that was encoded by the downstream exons (Fig. 4g).

3.5. Exon 8-skipped truncated kindlin-1 in vitro

To elucidate whether *KIND1* transcripts with in-frame deletion of exon 8 (transcript 1) express in living cells, we subcloned *KIND1* cDNA without exon 8 into pcDNA3.1V5-His vector (KIND1delex8).

Immunoblot analysis of lysates from HeLa cells transfected with KIND1delex8 showed a lower band than those of wild-type *KIND1*

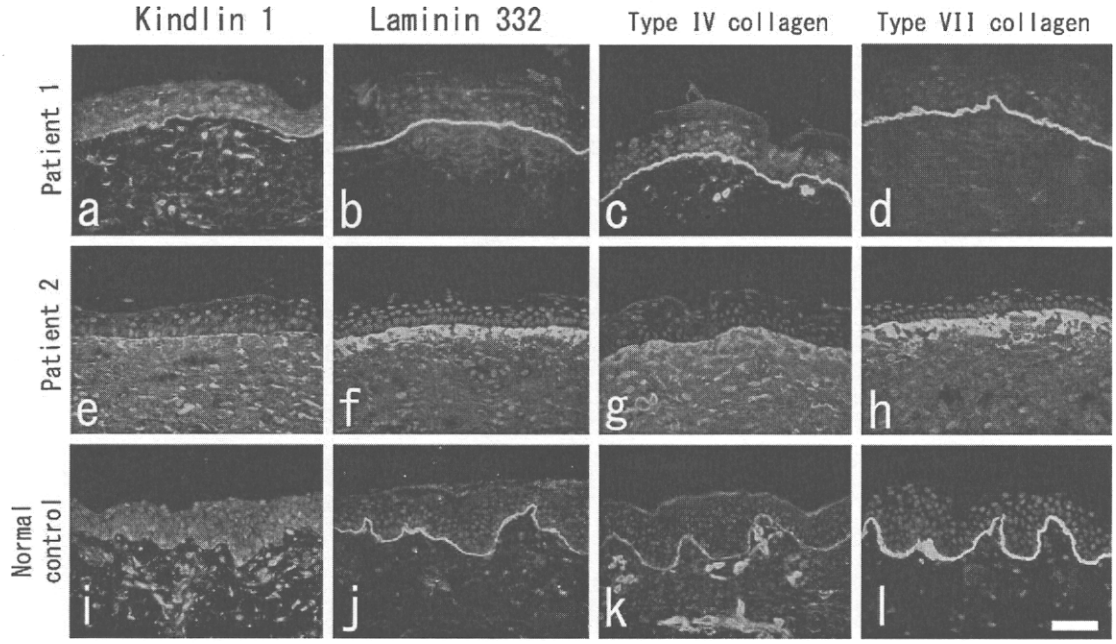

Fig. 3. Immunofluorescence analysis of skin specimens from KS with c.1089del/1089+1del. (a–d) Patient 1. (e–h) Patient 2 (a homozygote for c.1089del/1089+1del). (i–l) Normal control. Kindlin-1 labelling of skin specimens from Patients 1, 2 and the normal control show bright, linear staining at the DEJ as well as less intense labelling at the cell periphery in the basal keratinocytes (a, e, i). Thin, linear DEJ labelling with laminin 332, type IV collagen and type VII collagen is observed in skin samples from the present case (b–d) and normal control (j–l). Skin specimens from Patient 2 show interrupted or reduplicated DEJ (f–h) (bar: 50 μm).

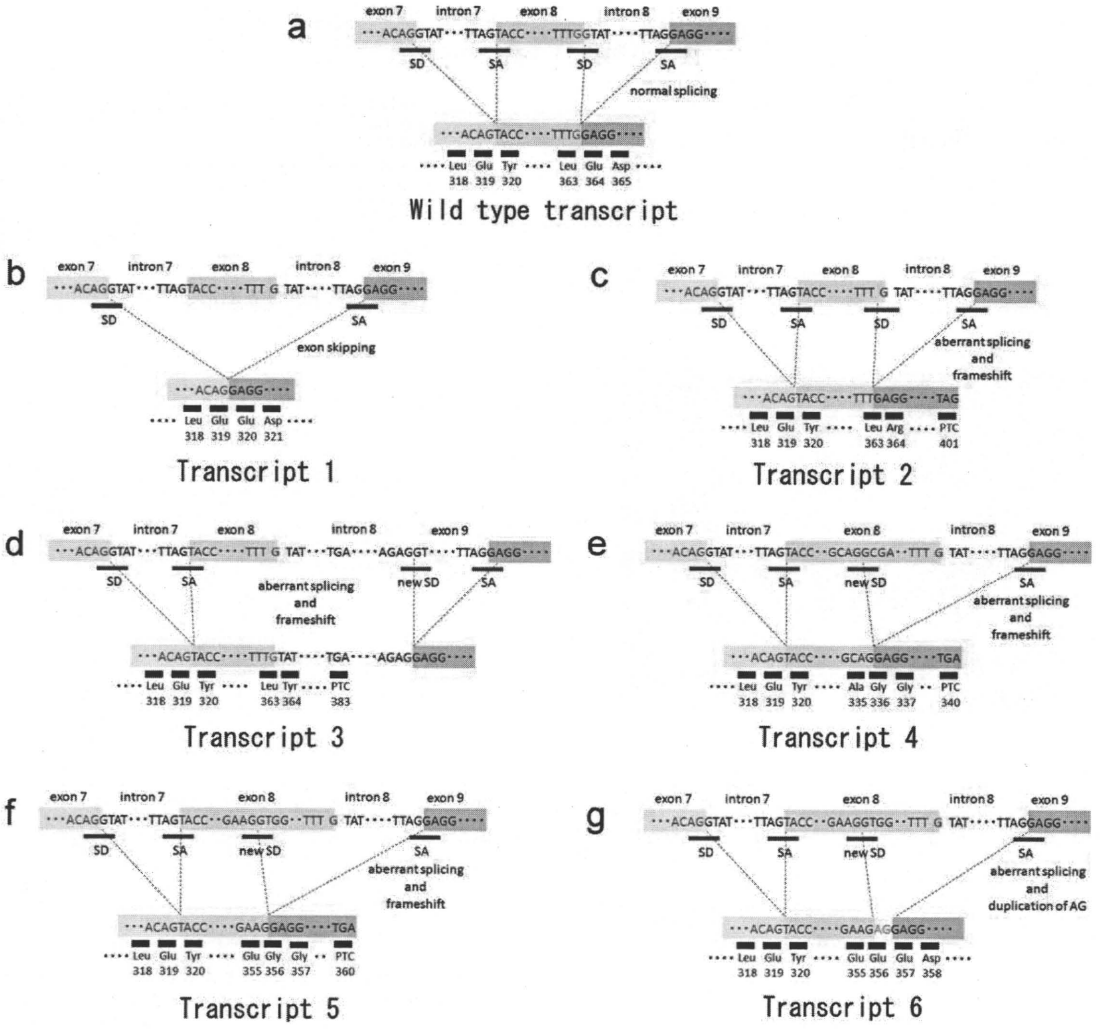

Fig. 4. Transcripts resulting from c.1089del/1089+1del. Wild-type (a) and mutant (b–g) sequences were subcloned in exon-trapping vector pSPL3 and transfected into HaCaT cells. Transcripts were derived from the pairing of vector and cloned splice signals. Boxes represent exons, blue underlines are splice sites (SD: splice donor site; SA: splice acceptor site) and black underlined regions are amino acids. Guanines at the exon 8/intron 8 boundary are in red. (a) The wild-type transcript contains exons 7, 8 and 9. (b) In transcript 1 (45 of 51 clones), exon 8 is skipped, and exon 7 is directly connected to exon 9. (c) In transcript 2 (1 of 51 clones), an exonic guanine is deleted at the 3′ end of exon 8, which results in frameshift and a premature termination codon (PTC). (d) In transcript 3 (1 of 51 clones), a new cryptic donor site within intron 8 is activated between nts 1089 + 240 and 1089 + 241. (e) Transcript 4 (2 of 51 clones) shows a new splice donor site within exon 8 between nts 1006 and 1007. (f) In transcript 5 (1 of 51 clones), another new splice donor site within exon 8 between 1066 and 1067 is activated. (g) Transcript 6 (2 of 51 clones) reveals a new splice donor site within exon 8 between 1066 and 1067 with duplication of nts 1065 and 1066 (AG).

cDNA (KIND1wt) (Fig. 5a). Total and activated β1 integrin was assessed as described previously [9]. Total surface β1 integrin detected by the mouse monoclonal anti-β1 integrin Ab (4B7R) was similar in the cells transfected with KIND1wt (Fig. 5b) and those transfected with KIND1delex8 (Fig. 5c). Localization of active β1 integrin labelling using the mouse monoclonal anti-β1 integrin Ab (clone 12G10) at focal adhesions was observed in the cells transfected with KIND1wt (Fig. 5d). However, active β1 integrin localized mostly at cytoplasms in the cells transfected with KIND1delex8 (Fig. 5e).

4. Discussion

Although the gene responsible for KS (*KIND1*) is now known, the complete KS pathomechanism has not been fully clarified. Our study revealed that the typical KS phenotype developed in KS patients with c.1089del/1089+1del possibly through defective β1 integrin activation even though kindlin-1 staining is positive as a result of the truncated protein.

KIND1 mutational analysis of Patient 1 identified one novel nonsense mutation c.1761T>A (p.Tyr587X). This nonsense mutation is thought to be targeted by nonsense-mediated mRNA decay (NMD). We also identified a recurrent mutation, c.1089del/1089+1del [7]. As two guanines exist at the exon/intron 8 boundary, it is impossible to determine whether the deleted guanine is from exon 8 or from intron 8 at the genomic DNA level. c.1089del, i.e. a guanine deletion from exon 8, predicts a frame-shifting change with leucine-97 as the first affected amino acid (p.Leu363fs) at the protein level [7]. Conversely, c.1089+1del, i.e. a guanine deletion from intron 8, should result in a splice donor site mutation [7]. The exon-trapping experiments in this study showed multiple transcripts produced by c.1089del/1089+1del. Exon 8 skipping produced a major transcript resulting from c.1089del/1089+1del (transcript 1, Fig. 4b).

Under immunofluorescence analysis, the skin specimens from Patient 1 and 2 tested positive for kindlin-1 (Fig. 3a and e). There are some reports describing KS patients with positive kindlin-1 staining [2,24]. From the data on transcripts from c.1089del/1089+1del, transcript 1 (in-frame deletion of exon 8, Fig. 4b) and

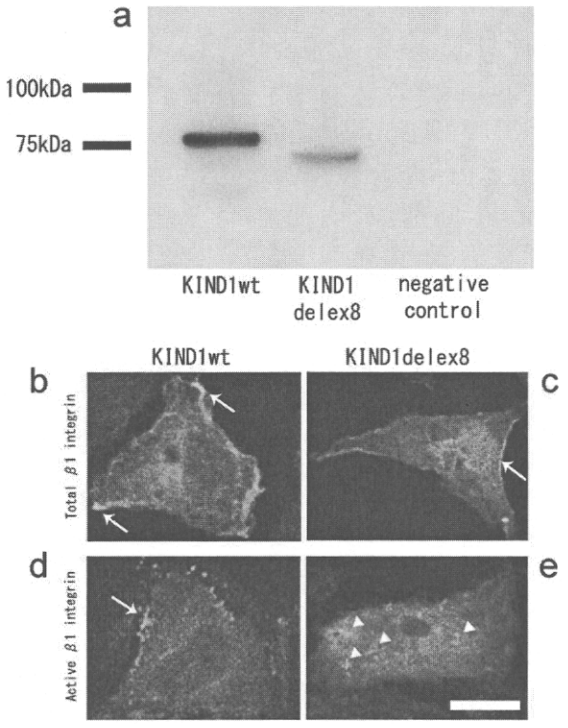

Fig. 5. Total and active β1 integrin expression in HeLa cells transfected with wild-type or mutated *KIND1* cDNA. (a) Immunoblot analysis of lysates from HeLa cells transfected with *KIND1* cDNA with (KIND1wt) or without exon 8 (KIND1delex8) confirms the expression of translated products (predicted sizes; 78 kDa and 74 kDa, respectively). pcDNA3.1V5-His vector without insert was used as negative control. (b, c) Total β1 integrin localization in HeLa cells transfected with KIND1wt (b) or KIND1delex8 (c). Only merged confocal microscopy images are shown. Total β1 integrin (red) localizes at focal adhesions (arrows) in both HeLa cells transfected with KIND1wt and those transfected with KIND1delex8. V5-tagged kindlin-1 is visualized with FITC-conjugated anti-V5 antibody. (d, e) Active β1 integrin labelling in HeLa cells transfected with KIND1wt (d) or KIND1delex8 (e). Active β1 integrin (red) localizes at focal adhesions (arrow) in the cells transfected with KIND1wt (d). In contrast, active β1 integrin is seen mostly in cytoplasms (arrowheads) in the cells transfected with KIND1delex8 (e) (bar: 5 μm).

transcript 6 (a new splice donor site between nts 1066 and 1067 with duplication of nts 1065 and 1066, Fig. 4g) can be regarded as responsible for positive kindlin-1 staining in our cases, because, in Patient 1, another allele harbouring c.1761T>A is predicted to be targeted by NMD. There is a possibility that the anti-kindlin-1 Ab utilized in this study (ab68041) reacts with both kindlin-1 and kindlin-2 because of the similar amino acids sequences between two proteins. However, the staining pattern of kindlin-2 in epidermis is reported as pan-epidermal membranous labelling but with no staining along the lower pole of basal keratinocytes in contact with the basement membrane [24]. In contrast, the normal human skin samples stained with ab68041 showed a linear labelling pattern at DEJ, which might indicate that the antibody is mostly against kindlin-1. Also, the expression level of kindlin-2 in skin is described to be almost parallel with that of kindlin-1 [24]. From these facts, we believe that the staining pattern we observed in this study reflects the expression of kindlin-1.

Even though truncated kindlin-1 expression in patient's skin is predicted from *in vitro* assay using cultured cells transfected with mutated *KIND1* cDNA, most of the clinical features of the patients with c.1089del/1089+1del are common to those of typical KS patients: generalized poikiloderma, skin atrophy especially on the dorsal aspects of the hands, and development of SCC and pseudosyndactyly [2]. This might be explained by impaired activation of β1 integrin in the cells transfected with mutated *KIND1* cDNA.

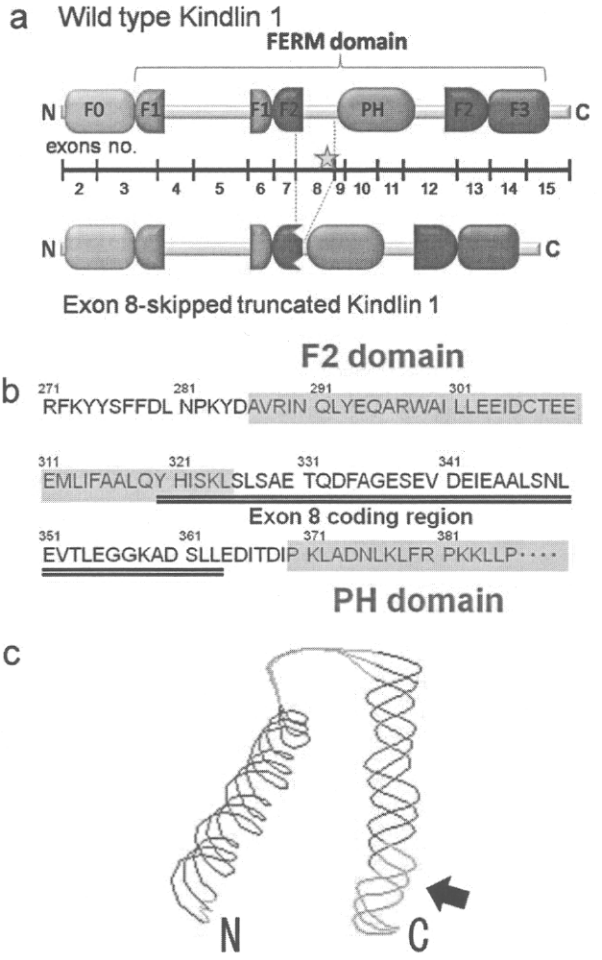

Fig. 6. Structural basis of exon-8-skipped truncated kindlin-1. (a) Schematic structure of wild-type and exon-8-skipped truncated kindlin-1. Kindlin-1 comprises the FERM domain, including F1, F2 and F3, flanked by the pleckstrin homology (PH) domain. A star indicates c.1089del/1089+1del at the exon 8/intron 8 boundary. (b) Exon 8 coding amino acids (black underline) are located in the F2 domain (red characters) and the unstructured area between the F2 and PH domains (blue characters). (c) Data on the 3D structure of the F2 domain of talin (PDB ID code: 2hrj) were obtained from the RCSB Protein Data Bank (http://www.rcsb.org/pdb/home/home.do). 3D imaging of the F2 domain of talin (amino acids 209-247) corresponding to that of kindlin-1 (amino acids 286–325) was done using Swiss-PdbViewer (ver 4.01). Exon 8 coding amino acids (green) in the F2 domain are located in the α helix (arrow).

The sequences of kindlin-1 are highly conserved and are very similar to those of the talin FERM domain, which is composed of F1, F2 and F3 [25] (Fig. 6a). F2 of kindlin-1 is interrupted by a large insert with a pleckstrin homology (PH) domain [26]. The exon 8 coding region is located in F2 and in an unstructured area between the F2 and PH domains (Fig. 6a). The 3D structure of the F2 domain indicates that the exon 8 coding amino acids in the F2 domain consist of the α helix (Fig. 6b and c). It is possible that exon-8-skipped truncated kindlin-1 leads to significant conformational change and loss of function and that truncated kindlin-1 expression resulting from c.1089del/1089+1del does not prevent KS development.

The immunohistochemical features of other DEJ molecules of Patient 1 were atypical. Previous studies revealed that antibodies against laminin-332, type IV collagen and type VII collagen shows a broad reticular staining pattern at the DEJ in typical KS patients (Fig. 3f–h) [3]. We were unable to observe such typical findings in the specimens of Patient 1, and only a thin linear labelling pattern was seen at the DEJ (Fig. 3b–d). A broad, reticular labelling pattern

at the DEJ is thought to correspond to marked reduplication of the lamina densa as a typical ultrastructural feature of KS patients [3]. Ultrastructural observation of Patient 1 also showed some lamina densa reduplication, but the extent was milder than that of typical KS (Fig. 1d). Limited reduplication of the lamina densa could explain the thin, linear labelling of laminin-332, type IV collagen and type VII collagen in Patient 1. However, the finding that skin specimens from Patient 2, who is homozygous for c.1089del/1089+1del, showed a broad reticular pattern at the DEJ (Fig. 3f–h) indicate that the presence of truncated kindlin-1 at the DEJ is not a cause of the linear thin immunofluorescence staining pattern of DEJ and the mild ultrastructural findings.

In summary, we have described a recurrent splice-site deletion mutation in *KIND1* in KS. The splice-site deletion produces multiple transcripts, most of which translatable into polypeptides that are encoded by the downstream exons. Although positive kindlin-1 staining in skin can therefore result from those transcripts, clinical manifestations of KS patients with c.1089del/1089+1del are as severe as those of KS with nonsense mutations because of defective integrin activation. This study, illumining the complicated pathomechanisms of KS, suggests that truncated kindlin-1 is functionally defective and cannot compensate for defects of KS.

Conflict of interest

The authors declare no conflict of interest.

Acknowledgements

We thank Prof John McGrath for his critical comments on the present case (Patient 1), Dr James R. McMillan and Mr Michael O'Connell for their proofreading, and Ms Yuko Hayakawa for her technical assistance. This work was supported by Health and Labour Sciences Research grants for Research on Measures for Intractable Diseases, from the Ministry of Health, Labour, and Welfare of Japan (to H.S.).

References

[1] Fine JD, Eady RA, Bauer EA, Bauer JW, Bruckner-Tuderman L, Heagerty A, et al. The classification of inherited epidermolysis bullosa (EB): report of the Third International Consensus Meeting on Diagnosis and Classification of EB. J Am Acad Dermatol 2008;58:931–50.

[2] Lai-Cheong JE, Tanaka A, Hawche G, Emanuel P, Maari C, Taskesen M, et al. Kindler syndrome: a focal adhesion genodermatosis. Br J Dermatol 2009;160:233–42.

[3] Shimizu H, Sato M, Ban M, Kitajima Y, Ishizaki S, Harada T, et al. Immunohistochemical, ultrastructural, and molecular features of Kindler syndrome distinguish it from dystrophic epidermolysis bullosa. Arch Dermatol 1997;133:1111–7.

[4] Hovnanian A, Blanchet-Bardon C, de Prost Y. Poikiloderma of Theresa Kindler: report of a case with ultrastructural study, and review of the literature. Pediatr Dermatol 1989;6:82–90.

[5] Yasukawa K, Sato-Matsumura KC, McMillan J, Tsuchiya K, Shimizu H. Exclusion of COL7A1 mutation in Kindler syndrome. J Am Acad Dermatol 2002;46:447–50.

[6] Jobard F, Bouadjar B, Caux F, Hadj-Rabia S, Has C, Matsuda F, et al. Identification of mutations in a new gene encoding a FERM family protein with a pleckstrin homology domain in Kindler syndrome. Hum Mol Genet 2003;12:925–35.

[7] Siegel DH, Ashton GH, Penagos HG, Lee JV, Feiler HS, Wilhelmsen KC, et al. Loss of kindlin-1, a human homolog of the *Caenorhabditis elegans* actin-extracellular-matrix linker protein UNC-112, causes Kindler syndrome. Am J Hum Genet 2003;73:174–87.

[8] Rogalski TM, Mullen GP, Gilbert MM, Williams BD, Moerman DG. The UNC-112 gene in *Caenorhabditis elegans* encodes a novel component of cell-matrix adhesion structures required for integrin localization in the muscle cell membrane. J Cell Biol 2000;150:253–64.

[9] Lai-Cheong JE, Parsons M, Tanaka A, Ussar S, South AP, Gomathy S, et al. Loss-of-function FERMT1 mutations in kindler syndrome implicate a role for fermitin family homolog-1 in integrin activation. Am J Pathol 2009;175:1431–41.

[10] Has C, Herz C, Zimina E, Qu HY, He Y, Zhang ZG, et al. Kindlin-1 is required for RhoGTPase-mediated lamellipodia formation in keratinocytes. Am J Pathol 2009;175:1442–52.

[11] Reese MG, Eeckman FH, Kulp D, Haussler D. Improved splice site detection in Genie. J Comput Biol 1997;4:311–23.

[12] Pertea M, Lin X, Salzberg SL. GeneSplicer: a new computational method for splice site prediction. Nucleic Acids Res 2001;29:1185–90.

[13] Baralle D, Baralle M. Splicing in action: assessing disease causing sequence changes. J Med Genet 2005;42:737–48.

[14] Buckler AJ, Chang DD, Graw SL, Brook JD, Haber DA, Sharp PA, et al. Exon amplification: a strategy to isolate mammalian genes based on RNA splicing. Proc Natl Acad Sci U S A 1991;88:4005–9.

[15] Schneider B, Koppius A, Sedlmeier R. Use of an exon-trapping vector for the evaluation of splice-site mutations. Mamm Genome 2007;18:670–6.

[16] Linard B, Bezieau S, Benlalam H, Labarriere N, Guilloux Y, Diez E, et al. A ras-mutated peptide targeted by CTL infiltrating a human melanoma lesion. J Immunol 2002;168:4802–8.

[17] Sapio MR, Posca D, Troncone G, Pettinato G, Palombini L, Rossi G, et al. Detection of BRAF mutation in thyroid papillary carcinomas by mutant allele-specific PCR amplification (MASA). Eur J Endocrinol 2006;154:341–8.

[18] Natsuga K, Nishie W, Shinkuma S, Arita K, Nakamura H, Ohyama M, et al. Plectin deficiency leads to both muscular dystrophy and pyloric atresia in epidermolysis bullosa simplex. Hum Mutat;31:E1687–98.

[19] Shimizu H, Fine JD, Suzumori K, Hatta N, Shozu M, Nishikawa T. Prenatal exclusion of pyloric atresia-junctional epidermolysis bullosa syndrome. J Am Acad Dermatol 1994;31:429–33.

[20] Natsuga K, Nishie W, Akiyama M, Nakamura H, Shinkuma S, McMillan JR, et al. Plectin expression patterns determine two distinct subtypes of epidermolysis bullosa simplex. Hum Mutat 2010;31:308–16.

[21] Laemmli UK. Cleavage of structural proteins during the assembly of the head of bacteriophage T4. Nature 1970;227:680–5.

[22] Goto M, Sato-Matsumura KC, Sawamura D, Yokota K, Nakamura H, Shimizu H. Tyrosinase gene analysis in Japanese patients with oculocutaneous albinism. J Dermatol Sci 2004;35:215–20.

[23] Nakamura H, Sawamura D, Goto M, Nakamura H, McMillan JR, Park S, et al. Epidermolysis bullosa simplex associated with pyloric atresia is a novel clinical subtype caused by mutations in the plectin gene (PLEC1). J Mol Diagn 2005;7:28–35.

[24] Lai-Cheong JE, Ussar S, Arita K, Hart IR, McGrath JA. Colocalization of kindlin-1, kindlin-2, and migfilin at keratinocyte focal adhesion and relevance to the pathophysiology of Kindler syndrome. J Invest Dermatol 2008;128:2156–65.

[25] Kloeker S, Major MB, Calderwood DA, Ginsberg MH, Jones DA, Beckerle MC. The Kindler syndrome protein is regulated by transforming growth factor-beta and involved in integrin-mediated adhesion. J Biol Chem 2004;279:6824–33.

[26] Goult BT, Bouaouina M, Harburger DS, Bate N, Patel B, Anthis NJ, et al. The structure of the N-terminus of kindlin-1: a domain important for alphaiib-beta3 integrin activation. J Mol Biol 2009;394:944–56.

DOI:10.1111/j.1600-0625.2010.01128.x
www.blackwellpublishing.com/EXD

Original Article

Protective effects of platinum nanoparticles against UV-light-induced epidermal inflammation

Yoko Yoshihisa[1], Ayumi Honda[1,2], Qing-Li Zhao[3], Teruhiko Makino[1], Riichiro Abe[2], Kotaro Matsui[1], Hiroshi Shimizu[2], Yusei Miyamoto[4], Takashi Kondo[3] and Tadamichi Shimizu[1]

[1]Department of Dermatology, Graduate School of Medicine and Pharmaceutical Sciences, University of Toyama, Sugitani, Toyama, Japan;
[2]Department of Dermatology, Graduate School of Medicine, Hokkaido University, Sapporo, Japan;
[3]Department of Radiological Sciences, Graduate School of Medicine and Pharmaceutical Sciences, University of Toyama, Sugitani, Toyama, Japan;
[4]Department of Integrated Biosciences, Graduate School of Frontier Sciences, University of Tokyo, Chiba, Japan
Correspondence: Tadamichi Shimizu, Department of Dermatology, Graduate School of Medicine and Pharmaceutical Sciences, University of Toyama, Sugitani, Toyama, Japan, Tel.: +81-76-434-7305, Fax: +81-76-434-5028, e-mail: shimizut@med.u-toyama.ac.jp

Accepted for publication 21 April 2010

Abstract: Intracellular reactive oxygen species (ROS) and apoptosis play important roles in the ultraviolet (UV)-induced inflammatory responses in the skin. Metal nanoparticles have been developed to increase the catalytic activity of metals, which is because of the large surface area of smaller particles. Platinum nanoparticles (nano-Pt) protected by poly acrylic acid were manufactured by reduction with ethanol. A marked increase in ROS production was observed in UV-treated HaCaT keratinocytes cell lines, while a decrease in ROS production was observed in nano-Pt-treated cells. Pretreatment of the cells with nano-Pt also caused a significant inhibition of UVB- and UVC-induced apoptosis. Furthermore, we found that mice treated with nano-Pt gel prior to UV irradiation showed significant inhibition of UVB-induced inflammation and UVA-induced photoallergy compared to UV-irradiated control mice. These results suggest that nano-Pt effectively protects against UV-induced inflammation by decreasing ROS production and inhibiting apoptosis in keratinocytes.

Key words: apoptosis – platinum nanoparticles – reactive oxygen species – skin – ultraviolet

Please cite this paper as: Protective effects of platinum nanoparticles against UV-light-induced epidermal inflammation. Experimental Dermatology 2010; **19**: 1000–1006.

Introduction

Skin is a major target for toxic insult by a broad spectrum of ultraviolet (UV) radiation that is capable of altering its structure and function. Photodamaged skin exhibits wrinkles, pigmented spots, dryness, and tumors. UV radiation has been reported to generate reactive oxygen species (ROS), such as singlet oxygen, superoxide radicals, hydroxyl radicals, and hydrogen peroxide, in a variety of cells (1), and intracellular ROS are thought to play an important role in UV-induced inflammatory responses in the skin. Both short-wavelength UVC (200–280 nm) and UVB (280–320 nm) as well as long-wavelength UVA (320–400 nm) produce ROS, which can lead to cell damage when the balance between the prooxidant stimuli and cellular antioxidant defenses is impaired (2,3).

The skin has a complex defense system of enzymatic and non-enzymatic components to counter the adverse biological effects of ROS. As the first defense, ROS are reduced by antioxidant enzymes, such as superoxide dismutase (SOD), catalase, and glutathione peroxidase, as well as endogenous and exogenous small molecules, including glutathione and vitamins C and E. When biomolecules are oxidized, they are repaired or replaced by biological protective systems. Nevertheless, biomolecules are gradually irreversibly oxidized, and accumulation of these biomolecules over time impairs biological functions, eventually leading to ageing and age-related diseases (4,5). Sunscreen use is a widely accepted method of primary prevention against skin cancer, sunburn, and photoageing. In fact, antioxidant compounds used in these products seem to function as protective substances against UV-induced ROS in the skin. Topical antioxidants, such as the flavonoid quercetin, have been reported to diminish UV radiation–mediated oxidative damage to the skin (6,7). Ascorbic acid (AA), which is the

Abbreviations: AA, ascorbic acid; IL, interleukin; MIF, macrophage migration inhibitory factor; MMP, mitochondrial membrane potential; nano-Pt, platinum nanoparticles; ROS, reactive oxygen species; TNF, tumor necrosis factor; UV, ultraviolet; LFLX, lomefloxacin hydrochloride.

Experimental Dermatology

most abundant antioxidant in the dermis, has exhibited a protective effect against oxidative stress.

Metal nanoparticles have been developed to increase the catalytic activity of metals because of the large surface area of smaller particles. Some noble metal nanoparticles are reducing catalysts that may be useful as antioxidants acting to reduce ROS in a living body. Nanotechnology is of interest because of the wide application of nanoparticles not only in material science and engineering but also in medical science and clinical use. Platinum nanoparticles (nano-Pt) protected by polyacrylic acid were recently manufactured by reduction with ethanol for 2 h (8). Nano-Pt are known to function as reductive catalysts; thus, they may be used as antioxidants to reduce ROS in living organisms. In fact, nano-Pt have the ability to scavenge O_2^- and H_2O_2, indicating that nano-Pt can act as a SOD/catalase mimetic (8). However, only a few studies have reported the antioxidant effects of nano-Pt in living organisms.

To elucidate the possible role of nano-Pt in UV-induced skin damage, we examined their protective effect on UV-induced ROS production and apoptosis using cultured keratinocytes. We also investigated the role of topically applied nano-Pt against UV-induced skin damage in mice.

Materials and methods

Reagents

Anti-Bcl-X_L monoclonal antibody (mAb), anti-Bax polyclonal antibody (pAb), anti-caspase-3 pAb, and anti-β-actin Ab were obtained from Santa Cruz Biotechnology, Inc.(Santa Cruz, CA, USA); nano-Pt were prepared as described previously (8). Nano-Pt gel was formulated by mixing 0.02% nano-Pt in water (corresponding to approximately 1 mM) with water and carboxyvinyl polymer (WAKO, Tokyo, Japan) (nano-Pt:water:carboxyvinyl polymer = 1:8.8:0.2) to yield a 0.002% w/w gel. Other reagents were of analytical grade.

Cell culture

HaCaT cells, an immortalized, non-tumorigenic human keratinocyte cell line (9), were maintained in DMEM (Invitrogen, Carlsbad, CA, USA) supplemented with 10% foetal bovine serum and 1% antibiotics at standard cell culture conditions (37°C, 5% CO_2 in a humidified incubator).

Mice

Eight-week-old male Balb/c mice were purchased from Japan Clea (Shizuoka, Japan). These mice were maintained under specific pathogen-free conditions. All experiments involving mice were performed in accordance with the guidelines for the care and use of laboratory animals at the Hokkaido University Graduate School of Medicine and University of Toyama.

UV irradiation

The UVA irradiation source was a FL20S/BLB fluorescent lamp (Clinical Supply, Tokyo, Japan) that emitted an energy spectrum with high fluency in the UVA region (300–430 nm), with a peak at 352 nm. A 6-mm-thick glass plate was used to block UVB emissions. The UVB light source was a FL20SE30 (Clinical Supply Co., Tokyo, Japan) fluorescent lamp that emitted 1.0 mW/cm^2 of UV radiation between 280 and 370 nm (peak 305 nm) at a distance of 25 cm, as measured by a UV radiometer (Torex Co., Tokyo, Japan). The UVC light source was a 615T8 (Sanyo Denki., Tokyo, Japan) fluorescent lamp that emitted 15 W of UV radiation between 190 and 280 nm (peak 254 nm) at a distance of 25 cm, as measured by a UV radiometer (Funakoshi Co., Tokyo, Japan).

Assessment of intracellular ROS

Intracellular ROS were measured using hydroethidine (HE) (Molecular Probes, Eugene, OR, USA) to detect intracellular superoxide (O_2^-) (10). HE is oxidized by O_2^- within the cells to produce ethidium bromide, which fluoresces when it intercalates into DNA. After 30 min of incubation following different treatments, the cells were stained with either 2 μM HE and incubated for 15 min at 37°C in darkness. Fluorescence emission of the resulting dyes was then analysed by flow cytometry.

Assay of DNA fragmentation

For the detection of apoptosis, the percentage of DNA fragmentation was assessed 24 h post treatment using the method of Sellins and Cohen (11) with minor modifications. In brief, approximately 3×10^6 cells were lysed using 200 μl of lysis buffer and centrifuged at 13 000 g for 10 min. Subsequently, DNA from each sample in the supernatant, and pellet was precipitated in 12.5% trichloroacetic acid (TCA) at 4°C overnight and quantified using the diphenylamine reagent after hydrolysis in 5% TCA at 90°C for 20 min. The percentage of fragmented DNA for each sample was calculated as the amount of DNA in the supernatant divided by the total DNA for that sample (supernatant plus pellet).

Assessment of early apoptosis and secondary necrosis

To determine the amount of early apoptosis and secondary necrosis, cells were collected 24 h post treatment and simultaneously stained with propidium iodide- and fluorescein isothiocyanate (FITC)-labelled annexin V, according to the instructions of the annexin V-FITC kit (Immunotech, Marseille, France) and finally, analysed with a flow cytometer (Beckman-Coulter EPICS XLTM) (12).

Measurement of mitochondrial membrane potential (MMP)

To measure changes in MMP, control cells and cells treated with nano-Pt (100 μM), HT, and a combination of both were collected at 6 h post treatment. The cells were then stained with 10 nM tetramethylrhodamine methyl ester (TMRM) (Molecular Probes, Eugene, OR) for 15 min at 37°C in phosphate-buffered saline (PBS) containing 1% FBS. The fluorescence of TMRM was analysed using flow cytometry (excitation at 488 nm; emission at 575 nm) (13).

Assay of UVB-induced inflammation and apoptosis *in vivo*

The mice were placed in individual compartments of specially designed cages, and their ears were exposed once to 350 mJ/cm^2 of UVB radiation. One group was treated with nano-Pt ointment on the earlobes (0.3 g on each earlobe) 24 h and immediately (two times) prior to UVB irradiation, while the other group was treated with carboxyvinyl polymer gel alone. The thickness of each ear was measured using a spring-loaded micrometre (Mitutoyo, Tokyo, Japan) to determine the baseline thickness. Ear swelling was calculated as the difference in ear thickness between the 24 h and the baseline values (14).

TUNEL assay

After 24 h, 350 mJ/cm^2 of UVB-irradiated mouse skin was obtained and analysed by TUNEL assay according to the manufacturer's instructions (R&D Systems). For statistical analysis, apoptotic cells were counted by light microscopy (100×) and expressed as the mean number (±SD) of apoptotic cells per section. Five random fields per section (one section per mouse, five mice per group) were analysed.

Assay of fluoroquinolone photoallergy

Fluoroquinolone photoallergy is inducible in Balb/c mice when they are sensitized by systemic administration of lomefloxacin hydrochloride (LFLX) (2 mg/0.2 ml, i.p.) followed by 12 J/cm^2 UVA irradiation of the shaved abdomen and challenged with systemic quinolone and UVA exposure of the earlobes (20 J/cm^2) (15). One group was treated with nano-Pt ointment on the earlobes (0.3 g on each earlobe) 24 h before and immediately (two times) prior to UVA challenge, while the other group was treated with carboxyvinyl polymer gel alone. Ear thickness was measured using an engineer's micrometre 6–10 days after the challenge and compared with ear thickness before the challenge.

Histological observation

Ears were fixed in 10% PBS-buffered formalin, and paraffin sections were stained with haematoxylin and eosin and examined by light microscopy to assess histological changes.

Northern blot analysis

Total cellular RNA was isolated from epidermis using the Isogen extraction kit according to the manufacturer's instructions. The epidermis was separated from the dermis by incubation in 0.5% dispase in RPMI-1640 at 37°C for 1 h. RNA was quantified spectrophotometrically, and equal amounts of RNA (10 μg) from samples were loaded on a formaldehyde-agarose gel. The gel was stained with ethidium bromide to visualize the RNA strands, and the RNA was transferred onto a nylon membrane. Fragments obtained by restriction enzyme treatments for tumor necrosis factor (TNF)-α, interleukin (IL)-1β, macrophage migration inhibitory factor (MIF), and GAPDH were labelled with [α-^{32}P]dCTP using a DNA random primer labelling kit. Hybridization was performed using the mouse MIF cDNA probe as described previously. The cDNA probes for TNF-α were 5′-TCTCATCAGTTCTATGGCCC-3′ (forward) and 5′-GGGAGTAGACAAGGTACAAC-3′ (reverse) and for IL-1β were 5′-CCCATACTTTAGGAAGACACGGATT-3′ (forward) and 5′-TCATGGGATGATGATGATAACCTGCT-3′ (reverse). The membrane was washed twice with 2× SSC (16.7 mM NaCl, 16.7 mM sodium citrate) at 22°C for 5 min, twice with 0.2× SSC containing 0.1% SDS at 65°C for 15 min, and twice with 2× SSC at 22°C for 20 min prior to autoradiography. The density of cytokine bands was normalized by the GAPDH intensities.

Western blot analysis

Cells were collected and washed with cold PBS. They were lysed at a density of 1 × 10^6 cells/50 μl of RIPA buffer (1 M Tris-HCl, 5 M NaCl, 1% Nonidet P-40 (v/v), 1% sodium deoxycholate, 0.05% SDS, 1 mM phenylmethyl sulfonyl fluoride) for 20 min. Following brief sonification, the lysates were centrifuged at 12 000 ***g*** for 10 min at 4°C, and the protein content in the supernatant was measured using the Bio-Rad protein assay kit (Bio-Rad, Hercules, CA, USA). Protein lysates were denatured at 96°C for 5 min after mixing with 5 μl SDS-loading buffer, applied on an SDS-polyacrylamide gel for electrophoresis, and transferred to nitrocellulose membranes. Western blot analysis was performed to detect Bcl-X_L, Bax, and caspase-3 expression using specific antibodies. Band signals were visualized on X-ray film using chemiluminescence ECL detection reagents (Amersham Biosciences, Buckinghamshire, UK) (16). Band density was quantified by a BIO-ID image analyzer, and the relative amounts of proteins associated with specific antibodies were normalized according to the intensities of β-actin.

Measurement of intracellular Pt content

The cells (1 × 10^7 cells) treated for 24 h with or without nano-Pt (100 μM) were collected by centrifugation, and the pellets were frozen. After thawing, each sample was placed in a glass vessel and reconstituted in nitric acid and hydrogen

peroxide (1:1). The solutions were evaporated to dryness on a hot plate and then, the residues were dissolved in dilute aqua regia (4 vol. %). Quantitative analysis of Pt for each solution was performed using inductively coupled plasma mass spectrometry (Model ELAN DRC II: Perkin Elmer SCIEX; Perkin Elmer Inc., Franklin, MA, USA).

Statistical analysis

Differences between the various treatments were statistically analysed using Student's *t*-test. For comparisons of multiple groups, one-way ANOVA was applied to the data. Furthermore, P values <0.05 were considered statistically significant. Data in the figures are shown as the mean ± SD of several experiments.

Results

Effects of nano-Pt on ROS production

We examined the effects of nano-Pt on UV-induced ROS production in keratinocytes. HaCaT cells were UV-treated with or without nano-Pt at different concentrations for 24 h, and flow cytometry with HE staining was used to detect ROS production in these cells. A marked increase in the production of O_2^- was observed 30 min after UV treatment in the cells. Nano-Pt at 100 μM concentration significantly inhibited each UV-induced O_2^- ($P \leq 0.001$) (Fig. S1). Therefore, we used nano-Pt at 100 μM concentration for next series of experiments. The percentage of cells producing O_2^- increased after UVA, UVB, and UVC irradiation dose dependently. Nano-Pt significantly inhibited UV-induced O_2^- [UVA 20 J/cm^2: 36.2 ± 2.1% ($P \leq 0.001$), UVB 60 mJ/cm^2: 26.0 ± 1.6% ($P < 0.05$), and UVC 60 mJ/cm^2: 42.7 ± 10.8% ($P \leq 0.001$)] (Fig. S1).

Effects of nano-Pt on UV-induced apoptosis

To investigate whether nano-Pt have the ability to protect against UV-induced apoptosis, HaCaT cells were UV-treated with or without nano-Pt (100 μM) for 24 h, and the effects were determined by evaluating DNA fragmentation in the cells. When these cells were pretreated with nano-Pt for 24 h, UVB- and UVC-induced apoptosis was significantly inhibited. On the other hand, nano-Pt had little effect on UVA-induced apoptosis, nano-Pt had only effective on 5 J/cm^2 UVA irradiation (Fig. 1). Annexin V-FITC-propidium iodide staining was used as a parameter for detecting apoptotic cell death, and the number of early apoptotic cells increased after UVB (20 and 40 mJ/cm^2) and UVC (20 and 40 mJ/cm^2) irradiation. Treatment with nano-Pt (100 μM) before UVB and UVC irradiation reduced the number of early apoptotic cells compared to UVB or UVC alone (Fig. 2). On the other hand, nano-Pt had no effect on UV-induced secondary necrosis.

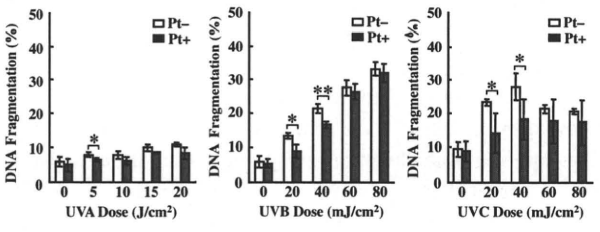

Figure 1. Effects of nano-Pt on ultraviolet-induced apoptosis. Cells were treated with UVA (5–20 J/cm^2), UVB (20–80 mJ/cm^2), and UVC (20–80 mJ/cm^2) with or without nano-Pt (100 μM) for 24 h. DNA fragmentation assay was performed after 24-h incubation at 37°C. Data are presented as mean ± SD (n = 5). *P < 0.05, **$P \leq$ 0.01. Data shown are representative of three independent experiments.

Expression of apoptosis-related proteins

Next, we evaluated changes in apoptotic marker proteins as a result of UV irradiation and exposure to nano-Pt (100 μM). The relative density of Bax, Bcl-X_L, and procaspase-3 to β-actin, calculated by integrating the density values of these three proteins, was similar in all the treated groups. The relative density of Bax to β-actin was 3.2 and 2.1 in samples irradiated with UVB and UVC, respectively. Nano-Pt decreased UVB- and UVC-induced Bax expression (UVB, 1.5; UVC, 1.7). The relative density of Bcl-X_L to β-actin was 0.08 in the UVB-irradiated samples. Furthermore, nano-Pt resulted in an increase in the UVB-induced Bcl-X_L expression (0.1) but did not alter the UVC-induced Bcl-X_L expression level. However, UVA irradiation did not alter Bax and Bcl-X_L expression levels. Expression of procaspase-3 decreased because of UVB and UVC irradiation and increased because of nano-Pt (Fig. 3). On the other hand, nano-Pt had no effect on Bax, Bcl-X_L, and procaspase-3 expression by UVA irradiation.

Effects of nano-Pt on Fas and the mitochondrial pathway

To examine the effects of nano-Pt on Fas externalization, cells were treated with or without 100 μM of nano-Pt for

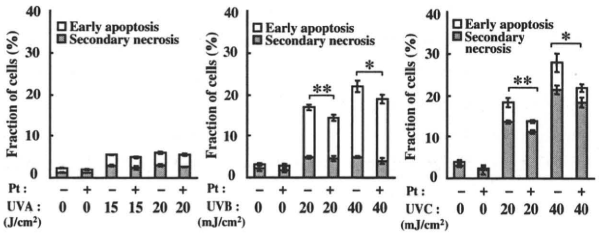

Figure 2. Effects of nano-Pt on ultraviolet (UV)-induced early apoptosis and secondary necrosis. Cells were treated with UVA, UVB, and UVC with or without nano-Pt (100 μM) for 24 h. Percentages of early apoptosis and secondary necrosis were analysed 24 h after UV treatment by flow cytometry. Data are presented as mean ± SD (n = 5). *$P \leq$ 0.05, **$P \leq$ 0.01. Data shown are representative of three independent experiments.

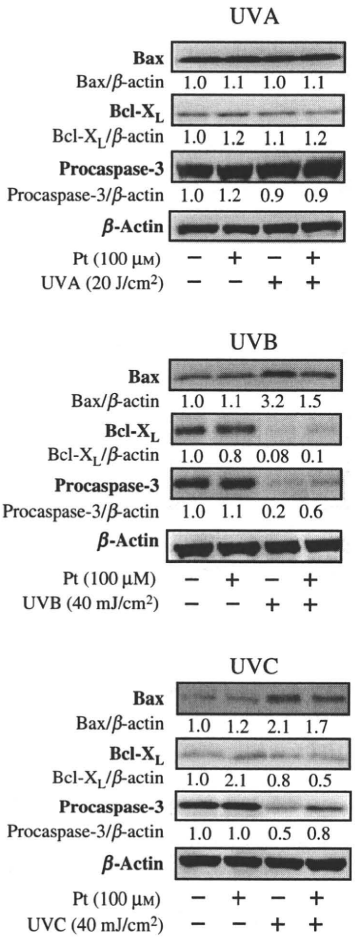

Figure 3. Ultraviolet-induced expression of apoptosis-related proteins. Immunoblot analysis of various apoptosis-related proteins in cells exposed to UVA, UVB, and UVC with or without nano-Pt (100 μM). Cell extracts were subjected to 5–20% SDS-PAGE and immunoblotted with antibodies against cleaved Bax, Bcl-X_L, caspase-3, and β-actin. Densitometry data, standardized by β-actin are presented below the band. Data shown are representative of three independent experiments.

24 h. Nano-Pt had no effect on UV-induced Fas production. Next, the effects of nano-Pt on the loss of mitochondrial membrane potential ($\Delta\Psi m$), which is an endpoint of apoptosis, were examined in HaCaT cells exposed to UV. Significant decrease in the loss of $\Delta\Psi m$ was observed (14.6 ± 3.1%; $P < 0.01$) when compared to UVB irradiation alone (Table 1).

Measurement of intracellular Pt content

When the intracellular content of Pt in samples was measured by inductively coupled plasma mass spectrometry, the values were 200 ng for treated cells and ≤0.05 ng for untreated control cells. Thus, intracellular incorporation of Pt was observed.

Table 1. Effects of nano-Pt endpoints of apoptosis

	Fas (%)	MMP (%)
Control	5.0 ± 0.1	5.0 ± 0.1
Pt + (100 μM)	5.1 ± 0.2	4.6 ± 0.4
UVA (20 J/cm^2)	21.6 ± 0.9	25.8 ± 1.6
Pt + UVA (20 J/cm^2)	20.7 ± 0.5	23.3 ± 2.0
UVB (40 mJ/cm^2)	15.6 ± 2.6	19.8 ± 1.2
Pt + UVB (40 mJ/cm^2)	13.2 ± 1.3	14.6 ± 3.1*
UVC (40 mJ/cm^2)	12.5 ± 2.8	9.6 ± 0.7
Pt + UVC (40 mJ/cm^2)	10.3 ± 1.7	9.2 ± 0.8

Cells were ultraviolet (UV) treated with or without nano-Pt (100 μM) for 24 h. The percentages of fraction of Fas positive cells are analyzed after UV treatment by flow cytometry using anti-Fas FITC antibody staining, and the percentages of loss of MMP are analyzed after UV treatment by flow cytometry using TMRM staining. The results are presented as the mean ± SD ($n = 5$).
*$P < 0.01$ vs UVB (40 mJ/cm^2).
MMP, mitochondrial membrane potential.

Effects of nano-Pt on UVB-mediated inflammation and apoptosis in mice

To present these results in an *in vivo* context, we analysed the role of nano-Pt ointment in UV-induced skin inflammation in mice. We assessed UVB irradiation–induced inflammation on the earlobes of mice. Twenty-four hours after 350 mJ/cm^2 UVB irradiation, the ear swelling in mice pretreated with nano-Pt gel was significantly decreased compared to that in UVB-irradiated control mice treated with carboxyvinyl gel polymer ($P < 0.01$) (Fig. S2). Immunochemical analysis demonstrated that a large number of TUNEL-positive cells were detected in the control mice after UVB irradiation, whereas few TUNEL-positive cells were detected in nano-Pt-treated mice ($P < 0.01$) (Fig. 5b,c). Thus, the nano-Pt-treated mice demonstrated a significantly smaller number of apoptotic cells than the control mice.

Effects of nano-Pt on photoallergy to LFLX plus UVA irradiation in mice

Subsequent studies were aimed to assess whether nano-Pt inhibit UVA-induced photoallergy. Fluoroquinolone photoallergy can be induced in Balb/c mice by sensitizing them by systemic administration of LFLX (2 mg/0.2 ml, i.p.), followed by 12 J/cm^2 UVA irradiation of the shaved abdomen, and posing a challenge using systemic quinolone and UVA exposure of the earlobes (20 J/cm^2). Significant ear swelling was observed in the positive control mice treated with carboxyvinyl polymer gel, but this response was inhibited in the earlobes of mice treated with nano-Pt gel prior to UVA irradiation ($P \leq 0.001$) (Fig. S3). Histological evaluation demonstrated that nano-Pt-treated mice had reduced cutaneous oedema, leucocyte infiltration, and hyperplasia even

on day 5 (Fig. S3). Northern blot analysis of the proinflammatory cytokine mRNA levels in the earlobes on day 5 showed decreased TNF-α, IL-1,β, and MIF expression in the nano-Pt-treated skin when compared to the positive control mouse skin (Fig. S3).

Discussion

UV irradiation of the skin results in a variety of injuries involving inflammatory and repair reactions, free radical reactions, and apoptosis. These injuries include immediate consequences, such as erythema and pigmentation, as well as delayed changes, such as cellular DNA mutations, hyperplasia, and carcinogenesis (17). ROS produced by UV radiation have the potential to damage critical cellular components, such as DNA, proteins, and lipids, eventually causing physical and chemical damage to skin tissues that may lead to cell death. To counteract oxidative injury, the skin is equipped with a network of enzymatic and non-enzymatic antioxidant systems, such as tocopherols and ascorbate polyphenols (18). This study demonstrated that treatment with nano-Pt reduced production of O_2^- in HaCaT cells before UV irradiation. Metal nanoparticles have been developed to increase the catalytic activity of metals because of the large surface area of smaller particles. Because nano-sized particles can reflect shorter wavelengths (UV light) (19), nanoparticles in the form of TiO_2 and ZnO have been used in sunscreen preparations to protect human skin physically. However, nano-Pt have been expected to protect human skin both physically and chemically owing to their SOD/catalase mimetic activity (8). Furthermore, compared to other metal nanoparticles, nano-Pt function as high reductive catalysts and may thus act as antioxidants to reduce ROS (8). Recently, Onizawa et al. demonstrated that treatment of alveolar-like A549 cells with nano-Pt inhibited cell death after exposure to a cigarette smoke extract. These results suggest that nano-Pt act as antioxidants that inhibit pulmonary inflammation induced by acute cigarette smoking (20). Furthermore, it has been demonstrated that nano-Pt prolonged the lifespan of worms, regardless of thermotolerance or dietary restriction (21). In this context, we suggest that nano-Pt are effective in reducing ROS production in UV-irradiated keratinocytes. Therefore, nano-Pt may have interesting anti-skin ageing properties.

Because DNA fragmentation, an endpoint of apoptosis, has been observed in human keratinocytes and HaCaT cells under certain conditions (22–24), we aimed at checking apoptosis-induction profile following different treatments using DNA fragmentation assay. The results revealed the occurrence of significant DNA fragmentation in HaCaT cells after UV irradiation. In this study, HaCaT cells irradiated with UVA, UVB, and UVC at different wavelengths demonstrated dose-dependent apoptosis following UVB and UVC exposure only, whereas no significant apoptosis was detected after UVA irradiation. Although UVA was shown to elevate intracellular superoxide production, it also induced delayed and sustained activation of extracellular signal-regulated kinase (ERK), which is apoptotic suppressor (25), and upregulation of the antiapoptotic protein Bcl-X_L by p38 MAPK activation (26). These simultaneous and opposing effects resulted in alleviation of the apoptotic stimulus. When HaCaT cells were irradiated with UVB and UVC in the presence of nano-Pt, UV-induced apoptosis was partially suppressed at 20 and 40 mJ/cm^2 in both cases. Because nano-Pt significantly attenuated superoxide formation in cells treated with UVA, UVB, and UVC but had no effect on peroxide formation, we concluded that superoxide plays an essential role in UVB- and UVC-induced apoptosis. It has been demonstrated that ROS increases the expression of cell surface Fas in human airway epithelial cells by promoting cytoplasmic transport of Fas (27). Thus, a putative mechanism of UVB- and UVC-induced apoptosis in HaCaT cells may involve accelerated recruitment of Fas on the cell membrane in response to elevated intracellular ROS, particularly superoxide, produced by UV irradiation. The apoptotic signal mediated by Fas guides the mitochondrial pathway and activation of caspase-3.

Similarly, our results demonstrated a significant increase in Fas expression and decrease in MMP in all UV-treated cells. On the other hand, a tendency for reduction in Fas expression and restoration of the decreased MMP content in the presence of nano-Pt was observed but was without statistical significance, except in case of UVB. When the Bcl-2 family proteins were measured, increased expression of the proapoptotic protein Bax and decreased expression of the antiapoptotic protein Bcl-X_L by UVB and UVC were reported. These effects were the opposite in the presence of nano-Pt. Furthermore, our data revealed caspase-3 activation by UV irradiation and its inhibition in the presence of nano-Pt. Therefore, the involvement of the mitochondrial caspase pathway and its modulation by intracellular superoxide in UV-induced apoptosis in HaCaT cells was confirmed. With respect to the localization of nanoparticles, Kiss et al. reported that TiO_2 nanoparticles cannot be uptaken by HaCaT cells (28). However, our results demonstrated the intracellular uptake of nano-Pt by HaCaT cells. Thus, we suggest that nano-Pt exerts protective effects because of their intracellular ROS scavenging activity.

The skin is continuously exposed to sunlight and environmental oxidizing pollutants; it is the preferred target of oxidative stress (29). Evidence suggests that signs of skin ageing, such as wrinkling, sagging, and actinic lentigines, may be associated with the cumulative oxidative damage incurred throughout our life. This study also demonstrates that nano-Pt gel applied topically on mouse skin protects against UVB-induced inflammation. Furthermore, we

demonstrated that nano-Pt have an antiapoptotic effect against UVB irradiation *in vivo*. UVB affects skin by inducing immunosuppression, premature skin ageing, inflammation, and cell death. Recent findings from our *in vivo* and *in vitro* observations suggest that nano-Pt can scavenge and inhibit inflammatory responses and apoptosis in the skin, which is caused by UVB exposure. Moreover, we found that nano-Pt gel was useful in mice with fluoroquinolone photoallergy. Fluoroquinolone photoallergy in mice is a model of photosensitivity dermatitis induced by UVA irradiation (30). Our results demonstrated that UVA-induced inflammation was clinically and histologically reduced by nano-Pt gel. Furthermore, proinflammatory cytokine levels in skin tissues decreased by nano-Pt treatment in mice with photoallergy. Sunscreens are recommended for protection against UV light–induced skin damage, but treatment of the skin with products containing antioxidant ingredients, such as tocopherols and ascorbate polyphenols, also be a useful strategy for the prevention of UV-mediated cutaneous damage. Broad-spectrum sunscreens are needed for protection against UVA. Therefore, it is suggested that nano-Pt demonstrating high antioxidant and antiinflammatory effects may have utility as a new class of sunscreens aimed at reducing ROS in the skin caused by UV exposure.

In conclusion, this study demonstrates that nano-Pt are effective in reducing UV-induced ROS and apoptosis and that topically applied nano-Pt effectively protects against UV-induced skin inflammation and photoallergy. Thus, we speculate that nano-Pt gel could be a useful sunscreen product for human skin therapy in the near future by providing effective protection against photo damage.

Acknowledgement

This research was supported by a Grant-in-Aid for research (No. 20591337) from the Ministry of Education, Science, and Culture of Japan.

Conflict of interest

The authors state no conflict of interest.

References

1 Peus D, Vasa R A, Meves A *et al.* H2O2 is an important mediator of UVB-induced EGF-receptor phosphorylation in cultured keratinocytes. J Invest Dermatol 1998: **110**: 966–971.
2 Ichihashi M, Ueda M, Budiyanto A *et al.* UV-induced skin damage. Toxicology 2003: **189**: 21–39.
3 Halliday G M. Inflammation, gene mutation and photoimmunosuppression in response to UVR-induced oxidative damage contributes to photocarcinogenesis. Mutat Res 2005: **571**: 107–120.
4 Bokov A, Chaudhuri A, Richardson A. The role of oxidative damage and stress in aging. Mech Ageing Dev 2004: **125**: 811–826.
5 Halliwell B. Antioxidant defence mechanisms: from the beginning to the end (of the beginning). Free Radic Res 1999: **31**: 261–272.
6 Saija A, Tomaino A, Trombetta D, Giacchi M, De Pasquale A, Bonina F. Influence of different penetration enhancers on in vitro skin permeation and in vivo photoprotective effect of flavonoids. Int J Pharm 1998: **175**: 85–94.
7 Casagrande R, Georgetti S R, Verri W A Jr, Dorta D J, dos Santos A C, Fonseca M J. Protective effect of topical formulations containing quercetin against UVB-induced oxidative stress. J Photochem Photobiol B 2006: **84**: 21–27.
8 Kajita M, Hikosaka K, Iitsuka M, Kanayama A, Toshima N, Miyamoto Y. Platinum nanoparticle is a useful scavenger of superoxide anion and hydrogen peroxide. Free Radic Res 2007: **41**: 615–626.
9 Boukamp P, Petrussevska R T, Breitkreutz D, Hornung J, Markham A, Fusenig N E. Normal keratinization in a spontaneously immortalized aneuploid human keratinocyte cell line. J Cell Biol 1998: **106**: 761–771.
10 Li F J, Kondo T, Zhao Q L *et al.* Enhancement of hyperthermia-induced apoptosis by a free radical initiator 2,2′-azobis (2-amidinopropane) dihydrochloride, in human histiocytic lymphoma U937 cells. Free Radic Res 2001: **35**: 281–299.
11 Sellins K S, Cohen J J. Gene induction by gamma-irradiation leads to DNA fragmentation in lymphocytes. J Immunol 1987: **139**: 3199–3206.
12 Hirano H, Tabuchi Y, Kondo T *et al.* Analysis of gene expression in apoptosis of human lymphoma U937 cells induced by heat shock and the effects of α-phenyl *N*-tert-butylnitrone (PBN) and its derivates. Apoptosis 2005: **10**: 331–340.
13 Zhao Q L, Fujiwara Y, Kondo T. Mechanism of cell death induction by nitroxide and hyperthermia. Free Radic Biol Med 2006: **40**: 1131–1143.
14 Lee E H, Faulhaber D, Hanson K M *et al.* Dietary lutein reduces ultraviolet radiation-induced inflammation and immunosuppression. J Invest Dermatol 2004: **122**: 510–517.
15 Tokura Y, Seo N, Yagi H, Furukawa F, Takigawa M. Cross-reactivity in murine fluoroquinolone photoallergy: exclusive usage of TCR Vbeta13 by immune T cells that recognize fluoroquinolone-photomodified cells. J Immunol 1998: **160**: 3719–3728.
16 Cui Z G, Kondo T, Ogawa R *et al.* Enhancement of radiation-induced apoptosis by 6-formylpterin. Free Radic Res 2004: **38**: 363–373.
17 Matsumura Y, Ananthaswamy H N. Toxic effects of ultraviolet radiation on the skin. Toxicol Appl Pharmacol 2004: **195**: 298–308.
18 Morganti P, Bruno C, Guarneri F, Cardillo A, Del Ciotto P, Valenzano F. Role of topical and nutritional supplement to modify the oxidative stress. Int J Cosmet Sci 2002: **24**: 331–339.
19 Sadrieh N, Wokovich A M, Gopee N V *et al.* Lack of significant dermal penetration of titanium dioxide (TiO_2) from sunscreen formulations containing nano- and sub-micron-size TiO_2 particles. Toxicol Sci 2010: **15**: 156–166.
20 Onizawa S, Aoshiba K, Kajita M, Miyamoto Y, Nagai A. Platinum nanoparticle antioxidants inhibit pulmonary inflammation in mice exposed to cigarette smoke. Pulm Pharmacol Ther 2009: **22**: 340–349.
21 Kim J, Takahashi M, Shimizu T *et al.* Effects of a potent antioxidant, platinum nanoparticle, on the lifespan of Caenorhabditis elegans. Mech Ageing Dev 2008: **129**: 322–331.
22 Woelfle U, Laszczyk M N, Kraus M *et al.* Triterpenes promote keratinocyte differentiation in vitro, ex vivo and in vivo: a role for the transient receptor potential canonical (subtype) 6. J Invest Dermatol 2009: **130**: 113–123.
23 Heinrich A, Balszuweit F, Thiermann H, Kehe K. Rapid simultaneous determination of apoptosis, necrosis, and viability in sulfur mustard exposed HaCaT cell cultures. Toxicol Lett 2009: **191**: 260–267.
24 Ayala F, Grimaldi E, Perfetto B *et al.* A 5-Aminolaevulinic acid and photodynamic therapy reduce HSV-1 replication in HaCat cells through an apoptosis-independent mechanism. Photodermatol Photoimmunol Photomed 2008: **24**: 237–243.
25 He Y -Y, Huang J -L, Colin CF. Delayed and sustained activation of extracellular signal-regulated kinase in human keratinocytes by UVA. J Biol Chem 2004: **279**: 53867–53874.
26 Bachelor M A, Bowden G T. Ultraviolet A-induced Modulation of Bcl-XL by p38 MAPK in Human Keratinocytes J Biol Chem 2004: **279**: 42658–42668.
27 Fujita A, Maruyama M, Araya J *et al.* Hydrogen peroxide induces upregulation of Fas in human airway epithelial cells via the activation of PARP-p53 pathway. Am J Respir Cell Mol Biol 2002: **27**: 542–552.
28 Kiss B, Bíró T, Czifra G *et al.* Investigation of micronized titanium dioxide penetration in human skin xenografts and its effect on cellular functions of human skin-derived cells. Exp Dermatol 2008: **17**: 659–667.
29 Thiele J J, Podda M, Packer L. Tropospheric ozone: an emerging environmental stress to skin. Biol Chem 1997: **378**: 1299–1305.
30 Tokura Y. Quinolone photoallergy: photosensitivity dermatitis induced by systemic administration of photohaptenic drugs. J Dermatol Sci 1998: **18**: 1–10.

Supporting Information

Additional Supporting Information may be found in the online version of this article:

Figure S1. Effects of nano-Pt on reactive oxygen species production.

Figure S2. Nano-Pt suppression of UVB-mediated inflammation in mice.

Figure S3. Nano-Pt suppression of photoallergy.

Please note: Wiley-Blackwell are not responsible for the content or functionality of any supporting materials supplied by the authors. Any queries (other than missing material) should be directed to the corresponding author for the article.

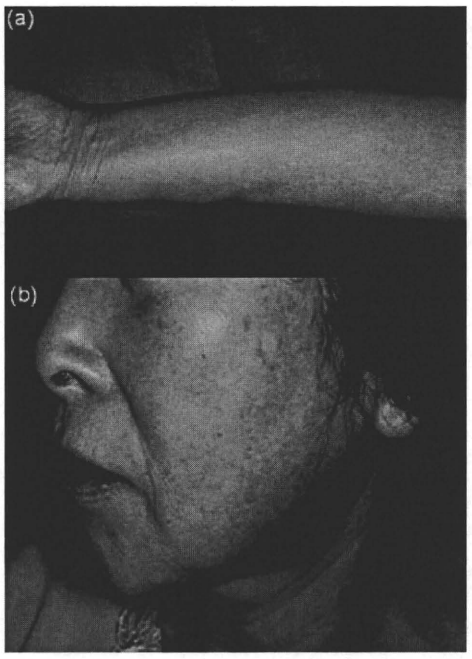

Fig. 1. Recurrent pruritic erythema on the left arm (a) and face (b).

Occupational contact dermatitis caused by asparagus

Contact Dermatitis 2010: 63: 54–54

Teruki Yanagi[1], Hiroshi Shimizu[1] and Tadamichi Shimizu[2]

[1]Department of Dermatology, Hokkaido University Graduate School of Medicine, Sapporo, and [2]Department of Dermatology, Toyama University Graduate School of Medicine, Toyama, Japan

Key words: asparagus; occupational contact dermatitis; patch test.

Case Report

A 67-year-old Japanese woman presented with a 2-year history of a recurrent pruritic erythema on the face, arms and hands (Fig. 1). She had worked in an asparagus cannery for 20 years. Her medical history indicated no evidence of atopic disease. The dermatitis cleared quickly with courses of anti-histamines and topical steroids but relapsed within days of returning to work. Rubber gloves were initially of benefit, but the pruritic eruption re-appeared when she touched her face with these gloves after working. She was patch-tested to a metals series and a freshly picked shoot of *Asparagus officinalis*. At both D2 and D3, the patch test with asparagus showed a strongly positive reaction (++), whereas all metals and white petrolatum were negative. Skin prick test with raw asparagus showed no skin reaction. Three normal healthy volunteer controls were negative on patch testing to asparagus. In light of the clinical observations and test results, occupational contact dermatitis to asparagus was diagnosed.

Discussion

Asparagus, one of the *Liliaceae* family members, is a vegetable that is cultivated worldwide and consumed when in season. Contact dermatitis to asparagus is rare (1–5). Several cases of allergic reactions by ingestion or inhalation of asparagus have been reported (6). Our patient, working in the cannery, had chronic/seasonally relapsing contact dermatitis to asparagus, which seems to be rare despite the widespread availability and consumption of asparagus. Although an association of contact dermatitis with other *Liliaceae* family members (garlic and onion) has frequently been reported as a result of occupational exposure (7), dermatologists should consider the potential of asparagus as an occupational allergen, particularly if allergic contact dermatitis occurs either chronically or seasonally.

References

1. Hausen B M, Wolf C. 1,2,3-Trithiane-5-carboxylic acid, a first contact allergen from *Asparagus officinalis* (Liliaceae). *Am J Contact Dermat* 1996: 7: 41–46.
2. Rademaker M, Yung A. Contact dermatitis to *Asparagus officinalis*. *Australas J Dermatol* 2000: 41: 262–263.
3. Rieker J, Ruzicka T, Neumann N J, Bielicky P, Homey B. [Type I and type IV sensitization to *Asparagus officinalis*]. *Hautarzt* 2004: 55: 397–398.
4. Rieker J, Ruzicka T, Neumann N J, Homey B. Protein contact dermatitis to asparagus. *J Allergy Clin Immunol* 2004: 113: 354–355.
5. Tabar A I, Alvarez-Puebla M J, Gomez B et al. Diversity of asparagus allergy: clinical and immunological features. *Clin Exp Allergy* 2004: 34: 131–136.
6. Volz T, Berner D, Weigert C, Rocken M, Biedermann T. Fixed food eruption caused by asparagus. *J Allergy Clin Immunol* 2005: 116: 1390–1392.
7. Hjorth N, Roed-Petersen J. Occupational protein contact dermatitis in food handlers. *Contact Dermatitis* 1976: 2: 28–42.

Address:
Teruki Yanagi
Department of Dermatology
Hokkaido University Graduate School of Medicine Sapporo
Japan
Tel: +81-11-716-1161
Fax: +81-11-706-7820
e-mail: yanagi@med.hokudai.ac.jp

The American Journal of Pathology, Vol. 177, No. 1, July 2010

DOI: 10.2353/ajpath.2010.091120

Epithelial and Mesenchymal Cell Biology

Self-Improvement of Keratinocyte Differentiation Defects During Skin Maturation in ABCA12-Deficient Harlequin Ichthyosis Model Mice

Teruki Yanagi,* Masashi Akiyama,* Hiroshi Nishihara,† Junko Ishikawa,‡ Kaori Sakai,* Yuki Miyamura,* Ayano Naoe,‡ Takashi Kitahara,‡ Shinya Tanaka,§ and Hiroshi Shimizu*

From the Department of Dermatology, Laboratory of Translational Pathology,† the Laboratory of Cancer Research,§ the Department of Pathology, Hokkaido University Graduate School of Medicine, Sapporo; and Tochigi Research Laboratories,‡ Kao Corporation, Ichikai, Haga, Tochigi, Japan*

Harlequin ichthyosis (HI) is caused by loss-of-function mutations in the keratinocyte lipid transporter ABCA12. The patients often die in the first 1 or 2 weeks of life, although HI survivors' phenotypes improve within several weeks after birth. In order to clarify the mechanisms of phenotypic recovery, we studied grafted skin and keratinocytes from *Abca12*-disrupted (*Abca12*$^{-/-}$) mice showing abnormal lipid transport. *Abca12*$^{-/-}$ neonatal epidermis showed significantly reduced total ceramide amounts and aberrant ceramide composition. Immunofluorescence and immunoblotting of *Abca12*$^{-/-}$ neonatal epidermis revealed defective profilaggrin/filaggrin conversion and reduced protein expression of the differentiation-specific molecules, loricrin, kallikrein 5, and transglutaminase 1, although their mRNA expression was up-regulated. In contrast, *Abca12*$^{-/-}$ skin grafts kept in a dry environment exhibited dramatic improvements in all these abnormalities. Increased transepidermal water loss, a parameter representing barrier defect, was remarkably decreased in grafted *Abca12*$^{-/-}$ skin. Ten-passage sub-cultured *Abca12*$^{-/-}$ keratinocytes showed restoration of intact ceramide distribution, differentiation-specific protein expression and profilaggrin/filaggrin conversion, which were defective in primary-cultures. Using cDNA microarray analysis, lipid transporters including four ATP-binding cassette transporters were up-regulated after sub-culture of *Abca12*$^{-/-}$ keratinocytes compared with primary-culture. These results indicate that disrupted keratinocyte differentiation during the fetal development is involved in the pathomechanism of HI and, during maturation, *Abca12*$^{-/-}$ epidermal keratinocytes regain normal differentiation processes. This restoration may account for the skin phenotype improvement observed in HI survivors. ***(Am J Pathol 2010, 177:106–118; DOI: 10.2353/ajpath.2010.091120)***

Harlequin ichthyosis (HI) (OMIM 242500) is one of the most severe genetic skin disorders, and its clinical features at birth include severe ectropion, eclabium, flattening of the ears, and large thick plate-like scales over the entire body.[1] Infants affected with HI frequently die within the early neonatal period, although an increasing survival rate for HI newborns has recently been highlighted.[2] In 2005, we and another independent research group identified mutations in the ATP-binding cassette transporter A12 (ABCA12) gene as the cause of HI.[3,4] We previously demonstrated that a severe ABCA12 deficiency causes defective lipid transport in lamellar granules in the upper spinous and granular layer keratinocytes, resulting in malformation of intercellular lipid layers at the granular/cornified layer interface and epidermal lipid barrier disruption resulting in HI phenotype.[3] We recently generated *Abca12*-disrupted (*Abca12*$^{-/-}$) mice by targeting *Abca12*, which closely reproduced the human HI phenotype and died soon after birth.[5] We tried systemic retinoid administration to the pregnant female mice as a form of fetal therapy, although no therapeutic effect was

Supported in part by a grant-in-aid from the Ministry of Education, Science, Sports, and Culture of Japan (Kiban B 20390304: to M.A.), a grant from Ministry of Health, Labor and Welfare of Japan (Health and Labor Sciences Research grants; Research on Intractable Disease: H21–047 and H22-177: to M.A.), a grant from ONO Medical Research Foundation (T.Y.) and a grant from Kanae Foundation for the promotion of Medical Science (T.Y.).

Accepted for publication February 26, 2010.

None of the authors declare any relevant financial relationships.

Supplemental material for this article can be found on *http://ajp.amjpathol.org*.

Address reprint requests to Masashi Akiyama, M.D., Ph.D., or Hiroshi Shimizu, M.D., Ph.D., Department of Dermatology, Hokkaido University Graduate School of Medicine, N15 W7, Kita-ku, Sapporo 060-8638, Japan. E-mail: akiyama@med.hokudai.ac.jp or shimizu@med.hokudai.ac.jp.